Analytical Approaches for the Segmentation of the Zebrafish Brain Vasculature

Elisabeth C. Kugler,[1,2,3,4,7] Andrik Rampun,[2,4,5] Timothy J. A. Chico,[2,3,4,6] and Paul A. Armitage[2,3,4,6]

[1]Institute of Ophthalmology, Faculty of Brain Sciences, University College London, Greater London
[2]Department of Infection, Immunity and Cardiovascular Disease, University of Sheffield, Medical School, Beech Hill Road, Sheffield, United Kingdom
[3]The Bateson Centre, Firth Court, University of Sheffield, Western Bank, Sheffield, United Kingdom
[4]Insigneo Institute for *in silico* Medicine, The Pam Liversidge Building, Sheffield, United Kingdom
[5]Posthumous Authorship
[6]Joint Senior Authors
[7]Corresponding author: *kugler.elisabeth@gmail.com*

With advancements in imaging techniques, data visualization allows new insights into fundamental biological processes of development and disease. However, although biomedical science is heavily reliant on imaging data, interpretation of datasets is still often based on subjective visual assessment rather than rigorous quantitation. This overview presents steps to validate image processing and segmentation using the zebrafish brain vasculature data acquired with light sheet fluorescence microscopy as a use case.

Blood vessels are of particular interest to both medical and biomedical science. Specific image enhancement filters have been developed that enhance blood vessels in imaging data prior to segmentation. Using the Sato enhancement filter as an example, we discuss how filter application can be evaluated and optimized. Approaches from the medical field such as simulated, experimental, and augmented datasets can be used to gain the most out of the data at hand. Using such datasets, we provide an overview of how biologists and data analysts can assess the accuracy, sensitivity, and robustness of their segmentation approaches that allow extraction of objects from images. Importantly, even after optimization and testing of a segmentation workflow (e.g., from a particular reporter line to another or between immunostaining processes), its generalizability is often limited, and this can be tested using double-transgenic reporter lines. Lastly, due to the increasing importance of deep learning networks, a comparative approach can be adopted to study their applicability to biological datasets.

In summary, we present a broad methodological overview ranging from image enhancement to segmentation with a mixed approach of experimental, simulated, and augmented datasets to assess and validate vascular segmentation using the zebrafish brain vasculature as an example.

Highlights

- Simulated, experimental, and augmented datasets provide an alternative to overcome the lack of segmentation gold standards and phantom models for zebrafish cerebrovascular segmentation.

CURRENT PROTOCOLS
A Wiley Brand

Current Protocols e443, Volume 2
Published in Wiley Online Library (wileyonlinelibrary.com).
doi: 10.1002/cpz1.443

- Direct generalization of a segmentation approach to the data for which it was not optimized (e.g., different transgenics or antibody stainings) should be treated with caution.
- Comparison of different deep learning segmentation methods can be used to assess their applicability to data. Here, we show that the zebrafish cerebral vasculature can be segmented with U-Net–based architectures, which outperform SegNet architectures.

Keywords: deep learning • light sheet • segmentation • vasculature • zebrafish

How to cite this article:
Kugler, E. C., Rampun, A., Chico, T. J. A., & Armitage, P. A. (2022). Analytical approaches for the segmentation of the zebrafish brain vasculature. *Current Protocols*, *2,* e443. doi: 10.1002/cpz1.443

INTRODUCTION

Abbreviations

BA	basilar artery
CNR	contrast-to-noise ratio
CtA	central artery
dpf	days post fertilization
FWHM	full width at half-maximum
GF	general filtering
hpf	hours post fertilization
LSFM	light sheet fluorescence microscopy
MMCtA	middle mesencephalic central artery
PMBC	primordial midbrain channel
ROI	region of interest
SE	Sato enhancement

Zebrafish as Preclinical Model in Cardiovascular Research

Vascular diseases are the leading cause of death worldwide (Feigin, Norrving, & Mensah, 2017; Lackland & Weber, 2015), whereas diseases of the central nervous system are associated with neurodegeneration, arteriovenous malformations, aneurysms, and stroke.

Zebrafish are commonly used to study embryonic development and disease due to their characteristics including high genomic similarity to humans, high progeny rates, and *ex utero* development (Bowley et al., 2021; Chico, Ingham, & Crossman, 2008; Gut, Reischauer, Stainier, & Arnaout, 2017). The availability of fluorescent transgenic reporter lines, combined with embryonic transparency, allows visualization of subcellular structures of interest with high specificity. For example, endothelial cells lining the vascular lumen can be visualized noninvasively *in vivo* (Lawson & Weinstein, 2002), allowing visualization of vascular anatomy with unprecedented spatial and temporal detail.

With the emergence of sophisticated microscopy techniques, such as light sheet fluorescence microscopy (LSFM), vascular information can not only be acquired with great anatomical detail but also over extended periods of time, such as hours to days (Huisken, Swoger, Del Bene, Wittbrodt, & Stelzer, 2004). Combining zebrafish fluorescent transgenic reporter lines and LSFM allows for acquiring data rich in anatomical depth, spatiotemporal resolution, and detail, enabling discovery and investigation of many biological processes (Bowley et al., 2021; Gut et al., 2017). Together, these advances mean that often it is no longer the experiments that are the limitations, but how to handle, analyze, and meaningfully interpret the acquired imaging datasets.

Challenges in Quantifying the Zebrafish Cranial Vasculature

Although certain characteristics of the cerebrovascular architecture may be obvious on visual inspection (such as missing or highly abnormal vessels), others may be too subtle for visual detection (such as diameter changes). Generally, 3D computational quantification of the vascular architecture is not only less labor-intensive but is also more comprehensive than manual assessments, providing measurements of volume, diameter, length, and branching (Kugler et al., 2022). Additionally, computational analysis is often more reproducible and sensitive than visual/manual assessment, requiring fewer animals.

In practice, before being able to quantify properties of objects/cells in 3D images, imaging data often need to be binarized, using a process called *segmentation*. In its simplest form, this first step toward computational data analysis extracts objects from grayscale or color images (*i.e., in semantic segmentation; instance segmentation could indicate individual vascular trees*). After segmentation, the image contains features of interest represented by a value of one, and everything else represented as zero. In the case of vascular segmentation, which separates vascular from nonvascular information, segmentation produces an output image where the pixels of the vasculature are represented by a value of one, and everything else by a value of zero. Even though vascular segmentation is critically important for quantitative vascular analysis, no existing study has examined how to validate a segmentation workflow in preclinical models such as zebrafish.

The main reasons for the lack of a robust and validated segmentation approach for the zebrafish cerebral vasculature are as follows:

i. Most research on zebrafish vasculature has focused on vascular development in the trunk, as trunk vessel formation shows a highly stereotypic growth pattern that is well characterized.
ii. Although the zebrafish brain vasculature is increasingly studied, its complex topology can present significant technical and experimental challenges for visualizing all vessels at the same level of detail.
iii. As endothelial cells are visualized in transgenic lines, a cross-sectional double-peak intensity distribution is displayed in lumenized vessels, whereas a single-peak distribution occurs in small or unlumenized vessels (Kugler, Chico, & Armitage, 2018). This means any analysis approach needs to either (a) be able to detect and discriminate these or (b) include a processing step that ensures all vessels have a single- or double-peak distribution. This is of particular importance when working with vessels with highly different diameters (such as 2-60 μm), as applying filters at a single scale across such a range is rarely feasible.
iv. LSFM is a relatively new technique, with commercial microscopes becoming available only in recent years.
v. Data acquisition with LSFM produces large datasets, requiring more computational resources for data handling, storage, and processing than other confocal imaging systems.
vi. Segmentation gold standards are lacking in preclinical models. In human medical imaging studies, segmentation gold standards usually take the form of expert manual measurements performed by a trained radiologist. However, there is no equivalent trained and qualified person in biological imaging. Additionally, due to the size and complexity of a zebrafish cranial vasculature dataset, extensive/accurate manual segmentation would be challenging and extremely time consuming (e.g., a single stack is typically around $1920 \times 1920 \times 400$ voxels, in the x, y, and z directions, respectively).
vii. Phantom models that replicate the zebrafish cranial vasculature, which could provide an alternative gold standard for validation, are not available.
viii. Due to the lack of previously validated segmentation approaches, benchmarks to compare new methodological improvements are unavailable.

Previous Work Aiming to Quantify the Zebrafish Cerebral Vasculature

Quantification of vessels in the left hindbrain was previously performed by Tam et al. (2012), whereas Chen et al. (2012) presented quantification of midbrain vascular segments. Both methods used confocal microscopy data and focused on a subregion rather than the whole brain vasculature. Tam et al. (2012) measured the vascular density and diameter after deconvolution using the commercial software Imaris. Chen et al. (2012) quantified vessel length, branching hierarchy (Strahler, 1952), the existence of loops, and vascular pruning events using the commercial software Neurolucida. However, neither study provided sufficient methodological detail to replicate and perform an in-depth assessment of their performance.

Recently, a machine learning segmentation approach was presented for the whole zebrafish embryonic vasculature using LSFM data (Daetwyler, Günther, Modes, Harrington, & Huisken, 2019). The method was trained on data from double-transgenic zebrafish, providing endothelial as well as luminal signals to ensure its robustness for single- and double-peak vessel profiles. As an additional luminal

signal (in this case a transgenic reporter line) is required to extract vascular information, the data load is doubled compared to that required for a single transgenic. Although this segmentation approach is promising, only visual assessment with no further validation of segmentation outcomes was performed.

Previously, Kugler and colleagues developed methods to enhance the cerebral vasculature in LSFM data using general filtering (GF) based on the application of median and rolling ball filters (Kugler et al., 2018) as well as by using a Hessian matrix–based enhancement, assuming local vessel tubularity, with the filter proposed by Sato and colleagues (Kugler, Plant, Chico, & Armitage, 2019; Sato et al., 1998). For the latter, local *image gradients* are described by the first image derivative and generalized into three dimensions by the Jacobian matrix, whereas the second derivative (*change of gradient*) is similarly represented by the Hessian matrix. To describe local curvature in the Hessian matrix, one can use nonzero vectors that change only by a scalar factor upon transformation, called *eigenvectors* (λ1, λ2, and λ3) and their respective magnitudes, i.e., *eigenvalues* (e1, e2, and e3). Using these eigenvectors and eigenvalues with the assumption that vessels are locally tubular/cylinder-like has inspired the development of vessel-specific filters to enhance vessel signals and reduce background. Two of the most widely used filters, originally developed for the medical field, are the *Frangi filter* (Frangi, Niessen, Vincken, & Viergever, 1998) and the *Sato enhancement filter* (Sato et al., 1998). The Sato enhancement filter uses the eigenvectors to enhance vessels assuming that vessels are locally a line, whereas the Frangi filter assumes them to be a tube. Sato enhancement is designed to use two eigenvalues to enhance tubes/lines, whereas the Frangi filter uses all three eigenvalues and considers sheets/plates, tubes/lines, and blobs/spheres. Additionally, the Frangi filter considers so called "*structureness*" describing gray level variations in images. Lastly, Frangi enhancement can work on dark vessels against a bright background and vice versa due to its use of absolute values, whereas Sato enhancement requires bright vessels against a dark background (for further information on mathematical definitions, the reader is referred to Frangi et al., 1998; Krissian, Malandain, & Ayache, 1998; Sato et al., 1998). Together, these vascular enhancement strategies are designed to increase contrast and gradient steepness between vascular and nonvascular signals prior to image segmentation. To this end, Kugler and colleagues (Kugler et al., 2019) investigated different image enhancement and subsequent segmentation methods, which were available in the open-source and widely-used Fiji image analysis software (Schindelin et al., 2012). These studies showed that for zebrafish brain vasculature data acquired with LSFM from fluorescent transgenic reporter lines, the best results were achieved applying Sato enhancement (Sato et al., 1998) at the scale of the examined vessels. This enhancement step was successfully followed by Otsu thresholding (Otsu, 1979) to achieve data binarization/segmentation, but again, no validation of the suggested approach was performed.

The above discussion proves that even though various approaches to segment the zebrafish brain vasculature exist, none have been validated and it is unclear how robust, sensitive, or accurate these approaches are. This lack of validation is particularly pressing as zebrafish are increasingly used to assess cerebrovascular changes upon disease, aging, and drug treatments (Bowley et al., 2021; Chico & Kugler, 2021). Thus, if segmentation approaches remain unvalidated, subtle biological phenotypes may be overlooked or falsely identified. Ideally, one would benchmark any new segmentation methodology against gold standard measurements covering a wide range of experimental situations including different vessel shapes, sizes, locations, data qualities/signal properties as well as image acquisition parameters acquired over a wide range of biological samples. As mentioned previously, expert manual segmentation is normally the accepted gold standard, but producing such data would be extremely time consuming, and it is unclear whether suitably qualified "experts" exist to perform such gold standard measurements. Therefore, comparing different segmentation methods can be used as a proxy to assess segmentation workflows.

Overview of Segmentation Validation Approaches

The lack of segmentation validation can be overcome by generating simulated data and manual measurements, along with studying datasets from groups subjected to experimental perturbation to challenge and assess segmentation performance. Below, we discuss different use cases that focus on the zebrafish cerebral vessels but describe approaches that can be widely used to assess segmentation outcomes when developing new segmentation workflows.

Together, this overview aims to (a) examine general approaches to assess segmentation quality and validate the suggested approaches, and (b) quantitatively address the lack of a segmentation gold standard for the zebrafish cerebrovascular architecture. The following are presented:

i. As phantom models with realistic optical properties are lacking for the zebrafish brain vasculature, computer-simulated digital tube models with realistic cerebrovascular and imaging properties (diameter, edge properties, signal distribution, and noise) can be used as proxies to test analysis step responses. As the underlying properties of these tubes are known, enhancement and segmentation outcomes can be validated against these known parameters. Although computer-generated datasets are commonly studied in the medical field, they are used less often in biomedical image analysis. Using such data, we show how to understand and optimize the Sato enhancement filter (Sato et al., 1998).

ii. Although it is not feasible to obtain a segmentation gold standard for the zebrafish cerebrovascular system by manual segmentation (standard image size 1920 × 1920 × 400 voxels, in the x, y, and z directions, respectively), manual measurement of vessel diameters in a small number of selected vessels can be performed. When selecting the respective vessels, these should include the typical range encountered in the data and, if possible, be distributed equally across the dorsal-to-ventral as well as anterior-to-posterior axis. These diameter measurements can then be used as a "gold standard" and compared to automated measurements obtained after enhancement and segmentation to provide an estimate of the accuracy of the enhancement and segmentation procedure.

iii. Assessing segmentation performance should include not only segmentation robustness but also whether true biological effects can be detected. We discuss three approaches for this:

   - To assess noise sensitivity, an experimental dataset with progressively decreasing image quality by controlled reduction of laser power, as quantified by the contrast-to-noise ratio (CNR), is produced. This dataset is further supplemented by a synthetic dataset generated with data augmentation.
   - To assess *segmentation sensitivity* to true biological changes in the cerebral vessels, segmentation is performed on data acquired in the same animal before and after exsanguination, expecting that this will result in a decreased vascular volume.
   - To further assess segmentation sensitivity, changes in the brain vascular volume during embryonic development from 3 to 5 days post fertilization (the standard way of referring to embryonic age) are quantified, as this is a period of growth and change that successful segmentation processes should detect.

iv. Even though general approaches to segmentation are often transferable to other types of datasets than those for which the approach was optimized, fine-tuning of individual steps, or parameters, is often required. Thus, to understand the generalizability of segmentation approaches, we demonstrate the degree to which segmentation developed for the transgenic *Tg(kdrl:HRAS-mCherry)*^{s916}, which has a high CNR (Kugler et al., 2019) and a vessel-specific expression pattern, could be applied to other transgenic lines, or whether further optimizations are required. The segmentation performance is assessed in the double-transgenic lines *Tg(fli1a:eGFP)*^{y1}, *Tg(kdrl:HRAS-mCherry)*^{s916} (Chi et al., 2008; Lawson & Weinstein, 2002), *Tg(fli1a:CAAX-eGFP),* *Tg(kdrl:HRAS-mCherry)*^{s916} (Gebala, Collins, Geudens, Phng, & Gerhardt, 2016), and *Tg(fli1a:LifeAct-mClover)*^{sh467}, *Tg(kdrl:HRAS-mCherry)*^{s916} (Savage et al., 2019), as using double transgenics allows direct comparison of segmentation outcomes, and the four transgenics examined are generally widely used in laboratories around the world. This shows that the segmentation approach is indeed transferable with respect to extracting the brain vasculature, but that further processing/improvement is required to remove nonspecific signals, such as those from the skin.

v. Lastly, due to the increasing importance and prevalence of deep learning (DL) methods in biological sciences, particularly in cerebrovascular segmentation of preclinical models (Daetwyler et al., 2019; Patera, Zippo, Bonnin, Stampanoni, &

Biella, 2021; Todorov et al., 2020), there is a need to understand DL methods and their applicability to biomedical imaging data. We highlight several DL methods and show how these can be assessed against each other to understand their applicability and performance; specifically, the original U-Net (Ronneberger, Fischer, & Brox, 2015), SegNet (Badrinarayanan, Kendall, & Cipolla, 2017), and three modified versions of the original U-Net architecture (dU-Net). Overall, we conclude that DL methods are indeed applicable to the zebrafish brain vascular architecture and that comparing DL methods against each other is useful and practical.

To facilitate the uptake and understanding of segmentation validation methods, we share example data where appropriate at zenodo.org: Simulated Tubes and Filter Responses (doi: 10.5281/zenodo.5898012), Decreasing Contrast-To-Noise Ratio (doi: 10.5281/zenodo.5910316), Exsanguination (doi: 10.5281/zenodo.5914725), and Development (doi: 10.5281/zenodo.5914749.

Together, general approaches to validate segmentation workflows applicable beyond the presented use case of the zebrafish brain vasculature are demonstrated. We believe these will help biologists and image analysts develop unbiased segmentation validation approaches for a wide range of applications.

ENHANCEMENT OF FILTER OPTIMIZATION AND VALIDATION

One common approach in vascular segmentation is to use vascular enhancement to improve image quality prior to binarization/segmentation. As mentioned above, these enhancement methods typically assume that vessels are locally a tube, i.e., a circular or ellipsoidal cross section that extends axially to form a tube. This shape-based assumption has led to various filters that enhance vessels relative to other structures, provided they have the expected tube-like properties, as is the case for the Sato, Frangi (Frangi et al., 1998, 1999; Sato et al., 1998), and other filters. However, these were traditionally implemented for clinical imaging modalities such as magnetic resonance imaging (MRI) where vascular contents are visualized. In this case, the vessel cross-sectional intensities are single peaks with radial Gaussian-like distributions. This contrasts with biomedical image analysis, such as zebrafish transgenic reporter lines or mouse antibody stainings, where the cells that make up the vessel walls—called *endothelial cells*—are visualized (Kugler et al., 2018; Todorov et al., 2020). This leads to a cross-sectional double-peak (or ring-shaped signal) intensity distribution in lumenized vessels, whereas unlumenized (often very small) vessels display single peaks (Kugler et al., 2018; Todorov et al., 2020). Although this could be addressed experimentally by performing microangiography, this is (a) laborious and (b) only shows perfused vessels. Thus, when applying vessel enhancement filters, one has to remember that these were implemented in clinical imaging rather than in fluorescence microscopy, i.e., for data with highly different signal properties and signal distributions.

Despite these major differences in data properties compared to the traditional applications where vessel content is imaged, the Sato enhancement (SE) filter—the filter that enhances lines/tubes based on eigenvectors—was previously shown to improve the quality of LSFM data from the zebrafish brain vasculature; this was quantified by the vessel-to-background CNR when applied at a scale size similar to the average vessel size. Moreover, in this work, approaches to measure CNR in the brain vasculature were demonstrated, and CNR measurements were generally found suitable for measuring the applicability of filters (Kugler et al., 2019).

In addition to CNR measurements, other vascular and image properties that enable assessment of filter responses include vessel diameters, edge properties, signal distribution, and noise. For example, to study the filter response at various vessel diameters, one can compare *in vivo* data from vessels with different diameters located at different anatomical positions throughout the brain, as exemplified in Figure 1A. When applying filters, these same vessels can be used to demonstrate the applicability of the filters, as shown here for SE, that successfully enhanced the displayed vessels (Fig. 1A′). A "successful" vessel enhancement filter is generally defined as the one that results in decreased background noise, more homogenous signals across the vessel, and an increased vessel-to-background CNR. To study the implementation of enhancement filters, image inversion can be used (Fig. 1B); for example, the theoretical assumption regarding SE is that it is only effective for bright vessels with a dark background. However, as computational implementations can differ from the original mathematical framework, testing both (dark-on-bright and bright-on-dark) scenarios can be useful. In this example, as expected, SE fails to perform vessel

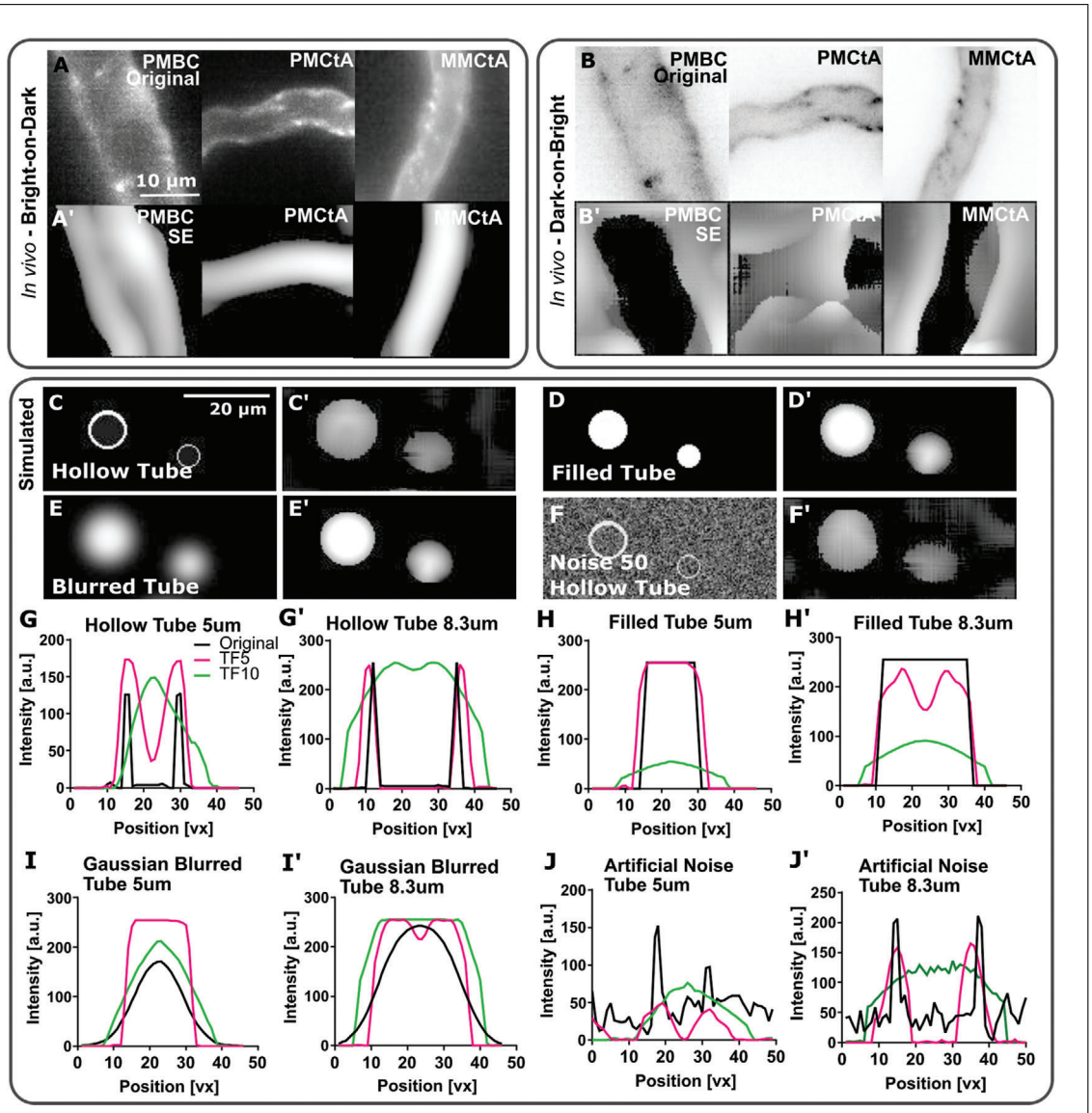

Figure 1 Vessel enhancement based on vascular tubularity and impact of the input shape. (**A**) Original data with bright vessels against a dark background. (**A′**) Data processed with Sato enhancement showed successful enhancement. (**B**) Inverted data with dark vessels against a bright background. (**B′**) SE was not able to perform after grayscale inversion. (**C,C′**) Applying SE to hollow tubes results in double-to-single peak conversion. (**D,D′**) Filling tubes with SE results in successful enhancement. (**E,E′**) SE enhancement results for Gaussian blurred tubes were similar to unblurred tubes. (**F,F′**) Addition of artificial Gaussian noise at level 50 did not significantly alter SE enhancement results.

enhancement on inverted images (Fig. 1B). Together, these tests show that the examined filter meaningfully enhances vessel enhancement, provided data are presented as bright-on-dark and applied at the scale of the desired vessels.

Vessel filters and subsequent segmentation outcomes are also affected by the input vessel shape and lumenization status:

- Lumenized, i.e., hollow tubes with double-peak intensity
- Unlumenized/unperfused, i.e., filled tubes with single-peak intensity

To test this, modeled tubes resembling the observed data can be produced computationally to create relevant "digital phantoms." These enable the study of filter impacts on vessels of different diameters, intensity distributions, and varying noise levels (see Materials and Methods for simulated tube details). Once simulated tubes are created, the filter of interest can then be applied to study the filter outputs visually using line ROIs to plot cross-sectional intensity distributions. For the use case presented here, SE was applied to simulated *hollow tubes*. Examining the

filter outcomes revealed that SE converted the tubes to filled tubes (conversion from double- to single-peak) upon enhancement at a scale approximately equal to the size of tubes (10 μm; Fig. 1C), suggesting that filled and unfilled vessels would be filtered similarly. The results obtained after enhancement of *filled* and *filled Gaussian-blurred* tubes were similar (Fig. 1D and 1E). Lastly, the addition of artificial Gaussian noise to the input images did not significantly affect enhancement (Fig. 1F), indicating the noise robustness of the filter. Together, such digital phantoms allow users to predict how filters might impact input data and whether satisfactory enhancement can be achieved before segmentation. These filters improve image quality, and the tubes can be considered "*filled*" following the enhancement step, thus making unlumenized and lumenized vessels equal for subsequent steps.

Other approaches could be to artificially fill all vessels after segmentation (i.e., a 3D hole-filling approach) or create vascular surfaces from the segmented objects and work with "empty" vessels. In essence, for quantification of vascular shapes or centerline extraction, vessels should have the same features (i.e., filled or unfilled), independent of the scale or properties, to allow all vessels to be analyzed in an unbiased fashion.

To gain further insight in an unbiased manner, cross-sectional intensity profiles can be plotted using line ROIs. For the presented use case, these profiles show that hollow-tube single-peak conversion is achieved when the filter is applied with the scale parameter at or larger than the tube diameter (Fig. 1G); however, filtering at a smaller scale leads to an increased edge response, with external and internal tube edges observed for tubes with double peak/ring profiles. This edge response increased upon filtering with a smaller sigma and was also observed for the other examined tubes (Fig. 1H-J). Thus, plotting cross-sectional intensity distributions before and after filtering provides additional insights into filter responses that might be overlooked upon visual data assessment.

By examining simulated tubes that are blurred and have additional noise, one can examine how filters respond to input data that more closely mimic the experimental data. As seen from the images and intensity profiles in Figure 1, there is a tendency for the simulated tube width to appear broader after enhancement. Any subsequent segmentation would need to be tuned for the correct vessel width (i.e., if there is a global and reproducible broadening during the enhancement step, this can be rectified during segmentation). It is important to note that when examining data in other vascular beds or species, where vascular diameters and signal profiles are different and possibly more variable than those in the zebrafish brain, alternative simulations would be required to ensure that the digital phantoms used to optimize the enhancement process represent the expected experimental data. This is likely to be the case when working with vessels spanning a large size range where multiple scales need to be integrated. Further details are available elsewhere (Chang, Huynh, Vazquez, & Salafia, 2013).

SEGMENTATION VALIDATION

Following image enhancement, the typical next step is image segmentation to binarize images for subsequent quantification. As there are a plethora of segmentation approaches, their discussion goes beyond the scope of this review; further information is available elsewhere (Khan, 2014; Kirbas & Quek, 2004; Lesage, Angelini, Bloch, & Funka-Lea, 2008; Moccia, De Momi, El Hadji, & Mattos, 2018; Renard, Guedria, Palma, & Vuillerme, 2020).

Before comprehensively discussing how to assess and validate a segmentation approach, we briefly want to touch upon two methods to assess the applicability of rapid segmentation to data: (a) visual assessment and (b) quantification using similarity metrics. *We present examples using the open-source software Fiji, but the general approaches equally apply to other image analysis software.*

For ***visual assessment***, it often suffices to observe the segmented data to determine whether over- (a nonvascular pixel classified as a vascular pixel, i.e., false positive) or undersegmentation (vascular pixels classified as background noise, i.e., false negative) occurred. Overlapping original images with segmented data is generally a suitable visual approach (e.g., Fiji: Image > Color > Merge Channels > select: C1 original and C2 segmented image). Examining data in detail and exploring them in 3D enables researchers to gauge whether, for example, there are global segmentation errors or whether certain regions are not well segmented.

For ***quantification using similarity metrics***, there are two steps to be examined: (i) the Fiji MorpholibJ Plugin (Legland, Arganda-Carreras, & Andrey, 2016), which allows quantification of image pixel overlap parameters such as the Dice coefficient, Jaccard index, or total pixel overlap; or (ii) comparing

image similarity parameters such as the sum of squared differences (SSD), sum of absolute differences (SAD), maximum absolute difference (MAD), mean square error (MSE), structural similarity (SSI), or mutual information (MI) (Matlab code: *https://github.com/ElisabethKugler/Matlab3D-ImageAnalysis/tree/main/ImageSimilarityMeasurement*).

Following these initial assessments, if the method appears to deliver a satisfactory enhancement and segmentation workflow, one can start to think about validating the approach more thoroughly. In the following sections, approaches to evaluate segmentation accuracy, robustness to noise, sensitivity to biological differences, and examinations of biological data (e.g., developmental data or different transgenic lines) are explored.

Segmentation accuracy

To identify whether a segmentation workflow is effective across the expected range of cerebral vessel sizes, segmentation *accuracy* has to be evaluated. This can be achieved by measuring vessel diameters after application of the enhancement and segmentation step and comparing those to the "gold standard" manual measurements. To gain additional insights into the role of image enhancement, different enhancement/segmentation workflows can be compared against each other. To showcase a comparative approach here, we compare data filtered with general [GF; median and rolling ball filters (Kugler et al., 2018)] or SE filters before segmentation, again using zebrafish brain vasculature data acquired with LSFM in the stable transgenic *Tg(kdrl:HRAS-mCherry)*^{s916} (Chi et al., 2008).

The first step is to establish a gold standard via manual measurements. Ideally, vessels spanning the full range of diameters observed in the data should be used; in the case of the zebrafish brain vasculature, this is 5-20 μm. Four vessels were chosen: the central artery (CtA), average diameter of 8.154±1.27 μm; the middle mesencephalic central artery (MMCtA), average diameter of 9.78±2.09 μm; the primordial midbrain channel (PMBC), average diameter of 11.14±1.68 μm; and the basilar artery (BA), average diameter of 22.28± 3.89 μm (n = 12; 3 dpf embryos). Importantly, selection of vessels will differ for different ages, vascular beds, visualizations (e.g., transgenics, or antibody stainings), or species, depending on the intended application.

As manual measurements are laborious and prone to bias, the full width at half-maximum (FWHM; code: *https://github.com/ElisabethKugler/Matlab3D-ImageAnalysis/tree/main/ImageProcessingTests*) of the cross-sectional intensity profile of the vessel is often used in the medical field to estimate the vessel diameter automatically. As this is less widely applied to preclinical models, comparing FWHM to the manual diameter measurements should provide meaningful insights into the overall applicability. We found no statistically significant differences (Fig. 2A; all vessels $p > 0.9999$) or error rates (CtA 1.44 μm, MMCtA 0.91 μm, PMBC 1.35 μm, and BA 3.83 μm). Using additional measures, such as Pearson Correlation and Bland-Altman analyses, can provide further insights into systematic errors that might otherwise be overlooked. When examining data, outliers might be encountered (Fig. 2A; unfilled arrowhead) and potential causes identified. For example, strong asymmetric cross-sectional intensity distributions (Fig. 2B) could lead to FWHM bias. Identifying this could then inform whether outlier exclusion is required or whether, for example, multidirectional FHWM measurement and averaging are needed; alternative approaches for vessel diameter measurements could be applied to address outliers (see reviews: Corliss, Mathews, Doty, Rohde, & Peirce, 2019; Lidayová, Frimmel, Wang, Bengtsson, & Smedby, 2017).

To further compare the impact of filters, estimates of the vascular diameters derived manually and using FWHM in original images can be compared with those derived from GF and SE after Otsu thresholding. This helps understand whether FWHM-, GF-, or SE-based diameter measurements and the corresponding manual measurements are comparable. Additionally, analyzing the intragroup coefficient of variation (CoV) provides insight into data variability. For example, in the data shown here, SE delivered more consistent results (Fig. 2C-G; CoV MMCtA manual 24%, FWHM 15%, GF 28%, and SE 17%; CoV CtA manual 11%, FWHM 42%, GF 57%, and SE 20%; CoV PMBC manual 12%, FWHM 42%, GF 57%, and SE 24%; CoV BA manual 14%, FWHM 29%, GF 13%, and SE 12%). Together with visual assessment (Fig. 2G-H; Videos 1 and 2), these steps indicate whether a segmentation workflow introduces artificial bias.

Segmentation robustness to noise

To assess segmentation *robustness to noise,* data with varying signal properties can be examined. To achieve this, two approaches are used for the presented use case: (a) acquisition

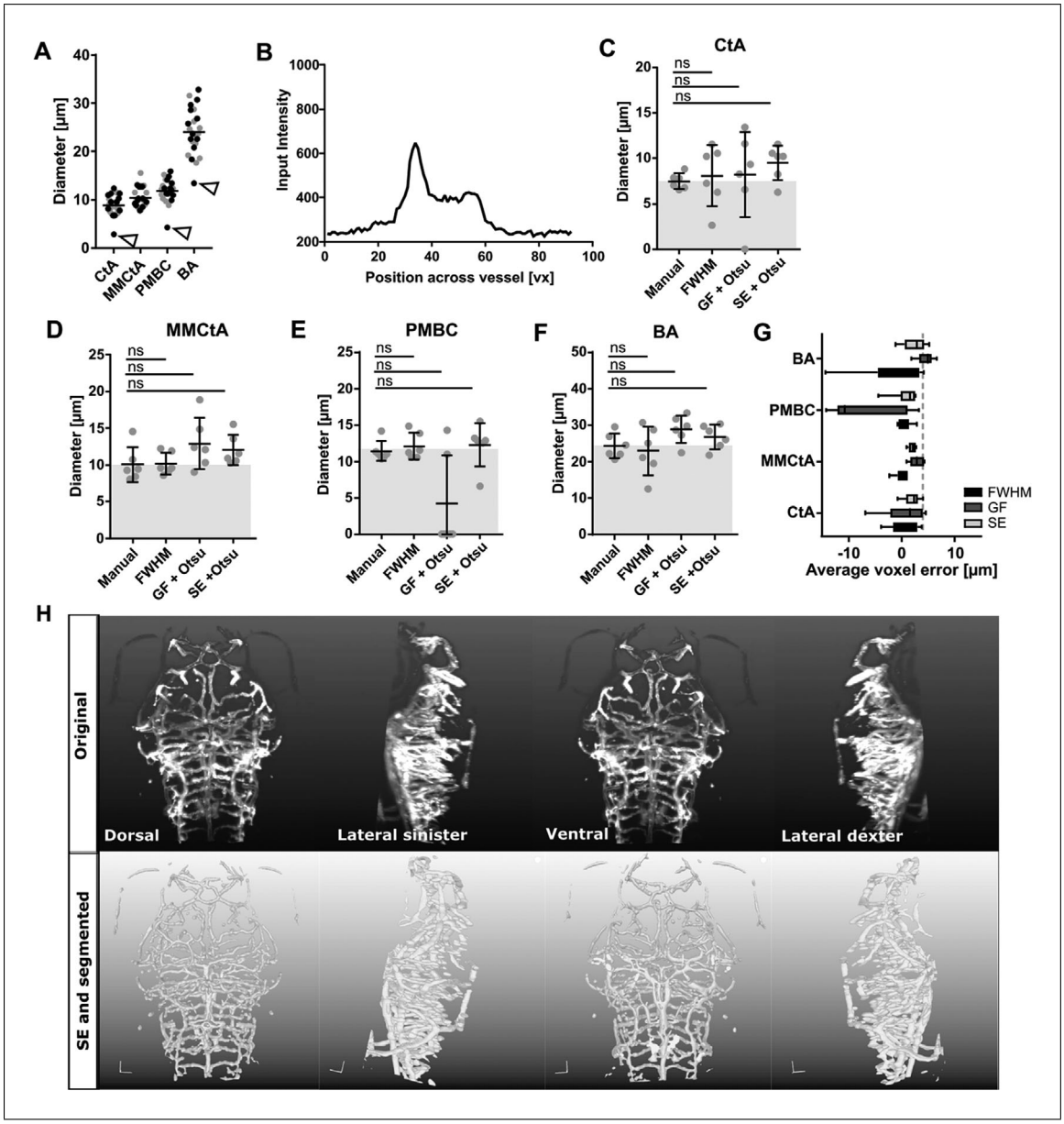

Figure 2 Validation of segmentation accuracy. (**A**) Comparing manual measurements (gray dots) to automated FWHM (black dots) showed good agreement. White arrowheads indicate outliers caused by skewed cross-sectional intensity distributions. (**B**) Comparison of manual measurements to FWHM, after GF with thresholding and SE with thresholding in the CtA (**C**), MMCtA (**D**), PMBC (**E**), and BA (**F**). Figures C-F show the Kruskal-Wallis test results. (**G**) Average voxel error is independent of vessel diameter (averaged n = 6; 3 dpf embryos). (**H**) Visual comparison of original data to images after SE and segmentation using 3D rendering.

of data with a systematic variation in image quality by consecutive imaging with reduced laser power (Fig. 3A-C) and (b) data augmentation by artificial noise addition (Fig. 3D-E), both followed by segmentation after GF and SE to again compare segmentation outcomes. For these experiments, image quality was characterized by the CNR between vascular and background signals, as described above and previously (Kugler et al., 2019).

To have an unbiased read-out when comparing segmentation outcomes, the 3D cerebrovascular volume can be quantified. When doing this for the example data examined here after GF or SE over the range of tested image qualities, no significant difference is encountered (Fig. 3F; $p = 0.3248$ and $p = 0.9981$, respectively). This suggests that both segmentation approaches are robust over a broad range of CNRs (CNR approx. 8-48). Again, assessing the CoVs of the volume measurements is a useful additional metric to assess variability (here: GF CoV: LP 1.2 18.76%, LP 0.8 14.63%, LP 0.4 17.56%; SE

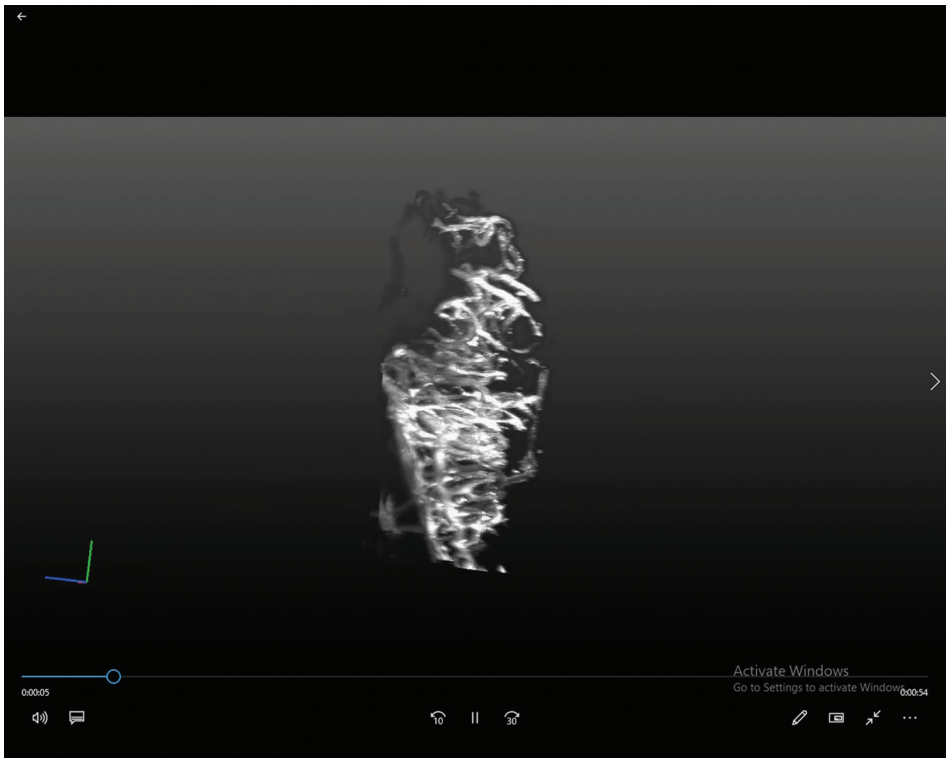

Video 1 Original image rendered in 3D. Video shows original 3D rendered 3 dpf *Tg(kdrl:HRAS-mCherry)*^{s916}.

Video 2 3D image rendered after SE and segmentation. Video shows 3D rendered 3 dpf *Tg(kdrl:HRAS-mCherry)*^{s916} after SE and segmentation.

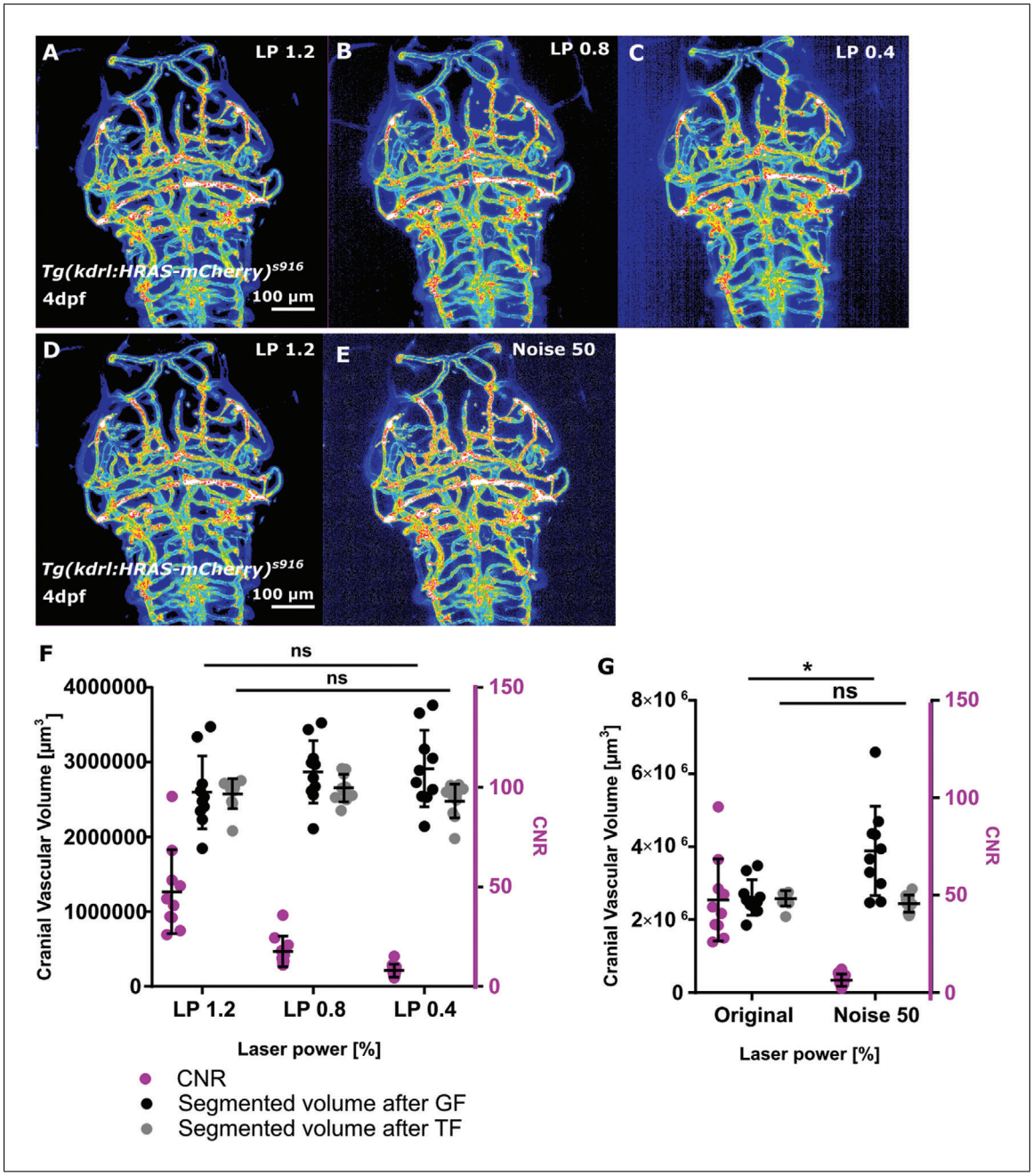

Figure 3 Validation of segmentation robustness. (**A-C**) Dataset with decreased image quality was produced by repeated image acquisition with reduced laser power (LP; 1.2%, 0.8%, and 0.4%). (**D-E**) Data augmentation was achieved by addition of noise to images of LP 1.2%.(**F**) In experimentally derived data, CNR (magenta) decreased as LP decreased. No statistically significant difference in vascular volume was observed after GF ($p = 0.3248$; black) or SE ($p = 0.9981$; gray) by LP reduction (n = 10; 4 dpf embryos; two experimental repetitions; one-way ANOVA). (**G**) In augmented data, CNR was also decreased (magenta). Vascular volume showed a statistically significant increase following GF ($p = 0.0247$) but not TF ($p > 0.9999$).

CoV: LP 1.2 7.81%, LP 0.8 6.97%, LP 0.4 9.14%).

Another suitable method is to use augmented data with increased noise and reduced CNR. However, as data augmentation is less widely applied in preclinical/biomedical image analysis, it first needs to be verified that the synthetic addition of noise correctly reproduces the noise distribution found in experimental data. Here, the CNRs as well as vascular volumes in the data were quantified with an experimentally derived CNR decrease and data with the addition of Gaussian noise. Analyzing this allows for assessing whether adding Gaussian noise can successfully produce data across a range of CNRs that are experimentally and biologically relevant (Fig. 3G). For the presented use case, the

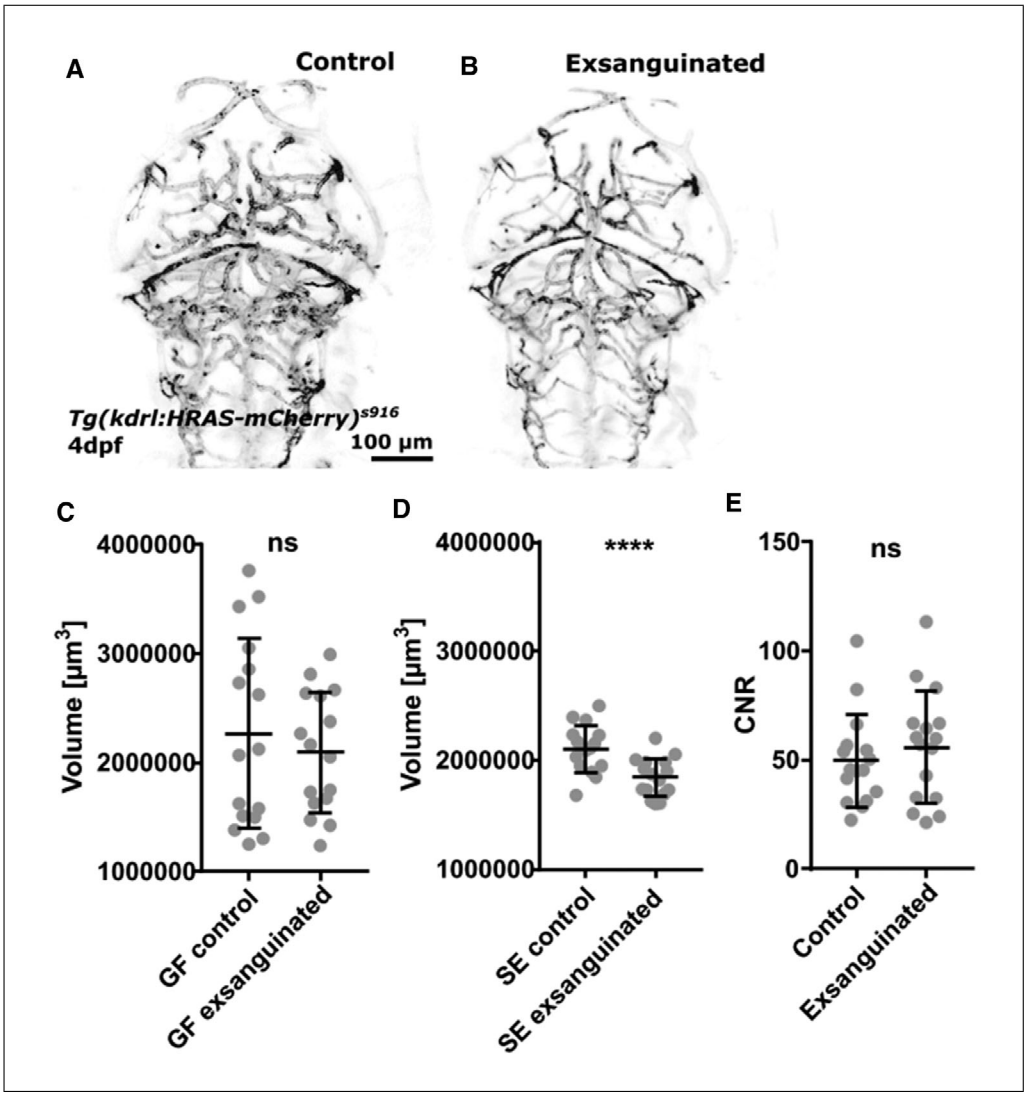

Figure 4 Validation of segmentation sensitivity. (**A-B**) Data were acquired before and after exsanguination. (**C**) Vascular volume was not statistically significantly different when comparing controls to exsanguinated samples after GF (p 0.2596; n = 16; 4 dpf embryos; two experimental repeats; paired t-test). (**D**) Vascular volume showed a statistically significant decrease when comparing controls to exsanguinated samples after SE ($p < 0.0001$; paired t-test). (**E**) CNR did not show a statistically significant change in the exsanguination procedure ($p = 0.0876$; paired t-test).

vascular volume was highly similar between the examined data, and when comparing GF- vs SE-based segmentation, GF was less robust across CNR levels. Together, experimental and augmented data with decreasing CNRs can be used to analyze segmentation robustness over a biologically relevant CNR range.

Segmentation sensitivity to biological differences

Segmentation *sensitivity* can be tested by comparing datasets with a predictable biological difference. For zebrafish, this can be achieved by imaging the same embryo before and after exsanguination, as blood loss will result in reduced vascular volume (Pestel et al., 2006; Fig. 4A and 4B). Again, using these data, a comparative approach for evaluating segmentation workflows can be applied, as shown for GF and SE, where the latter is able to extract a statistically significant reduction after SE ($p < 0.0001$; Fig. 4D; mean value difference – 8.05% decrease), whereas the former is not sensitive enough to do so (p 0.2596; Fig. 4C; mean value difference – 7.8% decrease). The volume CoVs for GF were 38.26% and 26.28% in controls and exsanguinated samples, respectively, whereas the SE CoVs were 10.22% and 9.65%, respectively. This again shows that examining the CoV is a useful measure of precision, in addition to other statistical analysis.

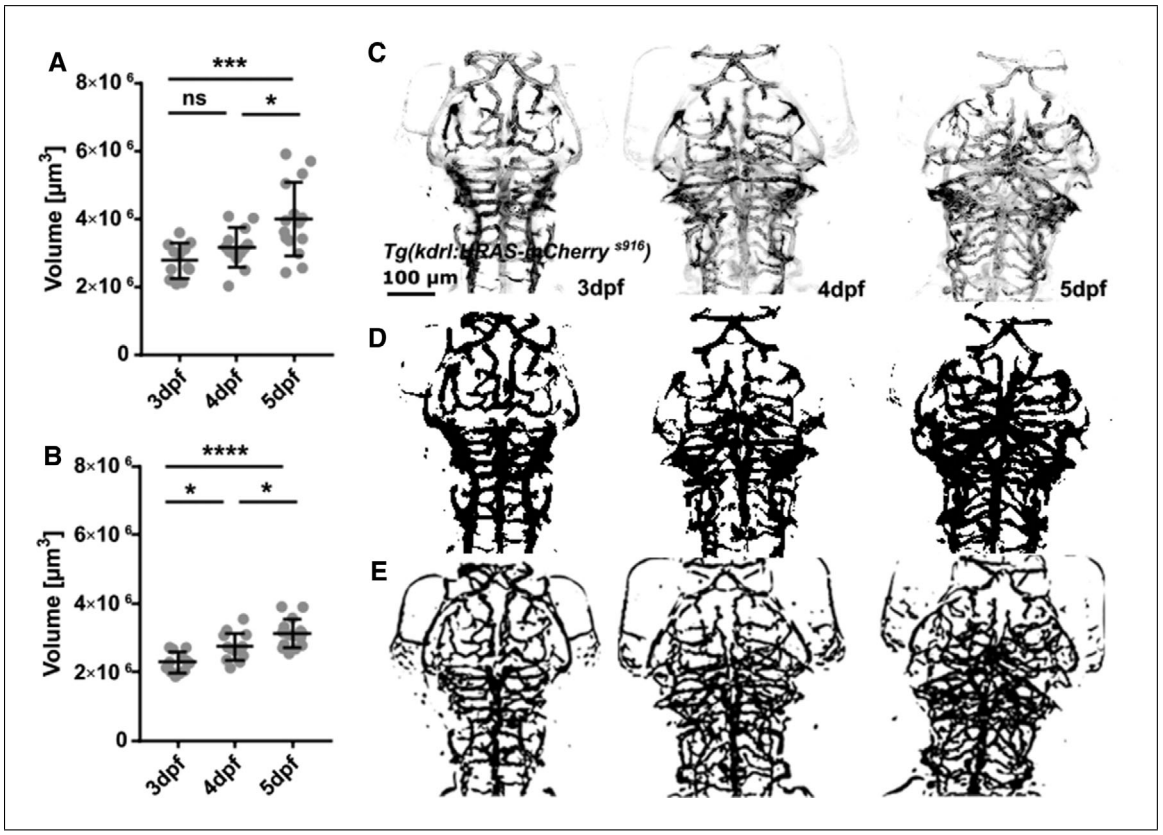

Figure 5 Application to quantify cerebral vascular volume. (**A**) Vascular volume showed a statistically significant increase after GF from 3 to 5 dpf ($p = 0.0009$; 3 dpf: n = 12; 4 dpf: n = 13; 5 dpf n = 15; two experimental repetitions; one-way ANOVA). (**B**) Vascular volume showed a statistically significant increase after SE from 3 to 5 dpf ($p < 0.0001$; one-way ANOVA). (**C**) Visual comparison of original data with segmented data after GF (**D**) and SE (**E**) indicating that SE delivered better results.

As procedures such as exsanguination are very invasive, we recommend using CNR measurements before and after such experimental manipulations to assess data quality alongside visual assessments (i.e., overall animal assessment, visual check for correct embedding, and ensuring that the same ROI is imaged). In the examined dataset, CNR measurements were conducted in the BA before and after exsanguination and revealed no statistically significant difference ($p = 0.0876$; Fig. 4E), indicating that data quality was largely unaltered and that the observed changes in the vascular volume were biological and not technical.

In summary, all the experiments discussed so far to study the accuracy, robustness, and sensitivity of the segmentation approaches show that combining simulated, experimental, and augmented data provides a powerful assessment of segmentation workflows. Furthermore, comparing different segmentation outcomes can be meaningful to elucidate the true accuracy and validity of segmentation workflows, e.g., determining if one approach is more accurate or robust than another.

Segmentation validation with developmental data

Although an initial examination of data with "severe" biological differences (such as those due to complete exsanguination) is reasonable, a more stringent test is to assess segmentation workflows further by trying to detect more subtle differences. For example, during embryonic cerebrovascular development, the vascular volume and complexity increase (Daetwyler et al., 2019). Here, we demonstrate segmentation of data from 3 to 5 dpf in zebrafish. We again compared the two example workflows, GF and SE. For both, a significant increase in the vascular volume was observed over time ($p = 0.0009$ and $p < 0.0001$, respectively; Fig. 5A and 5B). Again, the CoV was higher after GF (3 dpf 17.18%, 4 dpf 17.96%, 5 dpf 27.14%) than after SE (3 dpf 12.94%, 4 dpf 14.59%, 5 dpf 13.20%). As for any automated analysis step, additional visual assessment is recommended to confirm

whether segmentation is satisfactory (Fig. 5C) and comparable between samples.

Interestingly, the data indicate that during the studied developmental time frame, the mean vascular volume increase is approximately 12% (GF 3-4 dpf 11.42% and 4-5 dpf 12.59%; SE 3-4 dpf 11.99% and 4-5 dpf 11.39%), thus implying that accurate measurements are needed to extract subtle differences. As with all biological studies, it is important to consider the effect size expected between groups and how this relates to data analysis sensitivity (e.g., if the effect size is 30% between groups, it is likely that a crude analysis will be able to pick up differences; however, for an experiment with 7% effect size, a significantly more sensitive and accurate approach will be required unless group sizes can be greatly increased). Thus, comparing segmentation workflows, together with using the CoV to assess the precision of each method, again proved meaningful in deriving information on segmentation validity in data with subtle biological differences.

TRANSFERABILITY TO OTHER TRANSGENIC LINES

As most enhancement and segmentation approaches are optimized for one specific transgenic reporter line or antibody staining, it would also be useful to identify whether an approach developed based on a specific type of data would be generalizable to other types of data. Particularly in biomedical sciences, data may differ due to different visualization techniques (e.g., different transgenic reporter lines or antibody staining), animal ages, or experimental conditions. Understanding the limitations and transferability of a segmentation approach is pivotal when considering whether to apply it or reproduce a previously established approach.

To demonstrate this, the above workflow using SE and Otsu segmentation, which was optimized for the transgenic reporter line *Tg(kdrl:HRAS-mCherry)*^{s916} (Chi et al., 2008), is applied to other transgenic reporter lines. Specifically, double transgenics, namely (1) *Tg(fli1a:eGFP)*^{y1}, *Tg(kdrl:HRAS-mCherry)*^{s916} (Lawson & Weinstein, 2002), (2) *Tg(fli1a:CAAX-eGFP), Tg(kdrl:HRAS-mCherry)*^{s916} (Gebala et al., 2016), and (3) *Tg(fli1a:LifeAct-mClover)*^{sh467}, *Tg(kdrl:HRAS-mCherry)*^{s916} (Savage et al., 2019) are used. Based on the literature and our experience, we hypothesized that signals driven by the *fli1a* promotor would be more challenging to segment due to lower vascular specificity and higher image artifact levels, such as reflection from the skin (Fig. 6A and 6C). The double-transgenic reporter lines provide a useful comparison, as the signal from *Tg(kdrl:HRAS-mCherry)*^{s916} can be considered the gold standard.

Visual inspection demonstrates that actual vessels and diameters are accurately segmented but that additional nonvascular signals were segmented in the transgenic reporter lines driven by the *fli1a* reporter, which was not the case in *Tg(kdrl:HRAS-mCherry)*^{s916} (Fig. 6D-E). Using the cerebrovascular volume for comparison, a significant increase in the *fli1a* reporter in all the three examined lines can be observed ($p < 0.0001$ for all three; Fig. 6F-H). Even though the CoVs were moderate [17.28% *Tg(fli1a:eGFP)*^{y1}, 14.55% *Tg(fli1a:CAAX-eGFP),* 13.18% *Tg(fli1a:LifeAct-mClover)*^{sh467}], this exemplifies that further optimization and processing are needed to reliably extract vascular signals from transgenics other than those for which a segmentation workflow was developed and optimized. Importantly, depending on the data, generalization of a segmentation workflow will require optimization, especially when wanting to analyze data from samples with different ages, visualization techniques, and acquisition techniques, etc. The crucial point is to perform segmentation validation as described in this overview to assess segmentation outcomes quantitatively.

In the example shown here, further processing such as additional filtering or removal of peripheral or unconnected objects is clearly required. In such a case, where the original segmentation methodology is clearly not directly transferable to the new application, the whole optimization and validation process presented for *Tg(kdrl:HRAS-mCherry)*^{s916} would be repeated for each different transgenic line.

The presented proof-of-concept example shows that using double transgenics or double markers provides a valuable approach to (a) examine segmentation workflow outcomes, (b) identify/confirm optimal markers, and (c) study required optimizations for data beyond the original research question.

EXAMINATION OF DL METHODS

A vast range of DL methods exist for vasculature segmentation, with many outperforming conventional image analyses due to their ability to consider higher-level concepts (Litjens et al., 2017). Briefly, DL is a type of machine learning that uses levels of abstraction to learn from data; for example,

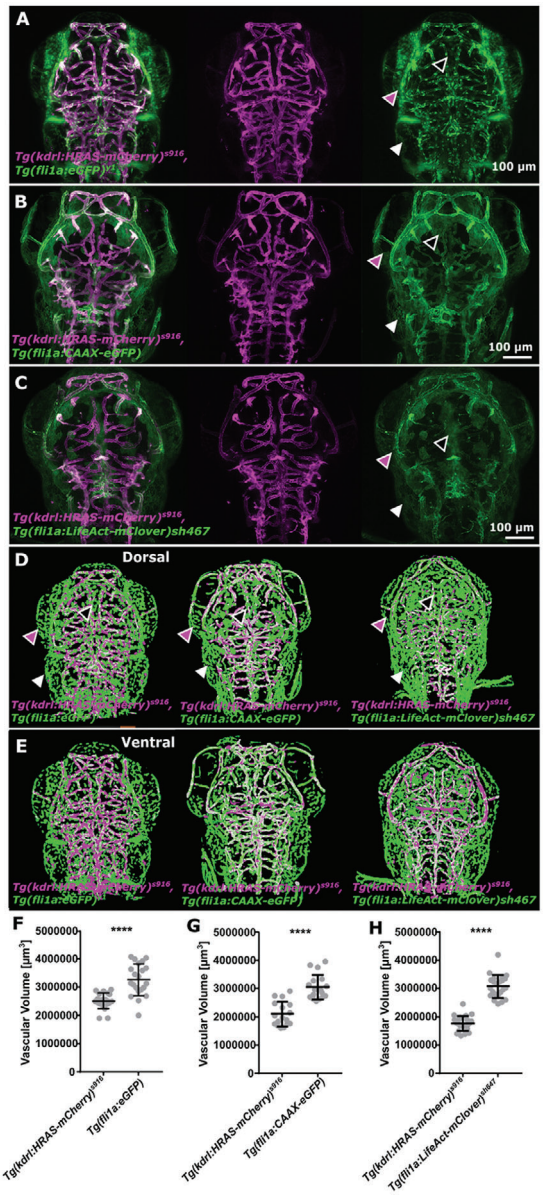

Figure 6 Segmentation of different transgenic lines. (**A-C**) In all three double transgenics [**(1)** Tg(fli1a:eGFP)^{y1}, Tg(kdrl:HRAS-mCherry)^{s916}, **(2)** Tg(fli1a:CAAX-eGFP), Tg(kdrl:HRAS-mCherry)^{s916}, and **(3)** Tg(fli1a:LifeAct-mClover)^{sh467}, Tg(kdrl:HRAS-mCherry)^{s916}] nonvascular signal was observed in the fli1a-driven transgenic (arrowheads). (**D-E**) Segmentation results of the three double transgenics showed nonvascular signals to be enhanced and segmented in the transgenics under the fli1a promotor. (**F**) Vascular volume in Tg(fli1a:eGFP)^{y1} was statistically significantly higher than in Tg(kdrl:HRAS-mCherry)^{s916} ($p < 0.0001$; n = 21; paired t-test). (**G**) Vascular volume in Tg(fli1a:CAAX-eGFP) was statistically significantly higher than Tg(kdrl:HRAS-mCherry)^{s916} ($p < 0.0001$; n = 17; paired t-test). (**H**) Vascular volume in Tg(fli1a:LifeAct-mClover)^{sh467} was statistically significantly higher than Tg(kdrl:HRAS-mCherry)^{s916} ($p < 0.0001$; n = 23; paired t-test).

neural networks mimic how the brain works, which informs subsequent data analysis (LeCun, Bengio, & Hinton, 2015; Moen et al., 2019). Training an algorithm to learn from data to perform a classification task, such as segmentation, is particularly useful when working with biological data where the task is more complex, and the answers are not easily obtainable. Thus, with its expansion and widening uptake, DL has also found its way into biological sciences as well as cerebrovascular segmentation of preclinical

models (Daetwyler et al., 2019; Patera et al., 2021; Todorov et al., 2020).

However, to establish a DL approach, one also needs to consider accuracy. In the following example, we provide an overview on how to assess the applicability of supervised DL approaches, where the networks learn from a labeled dataset (i.e., the "ground truth" can be derived from manual labeling or the current segmentation gold standard), for image segmentation where DL was previously not used. To achieve this, the DL networks learn on "*training data*" (in this case, the "ground truth" data segmented with the SE-based approach) and are tested on separate data called "*test data*," eventually performing their intended tasks on *new data* once the DL model parameterization has been established from the training data.

Reproducibility and variability of DL are often problematic. This could be due to the lack of the following three components: (i) DL framework description, (ii) assessment of variability, and (iii) segmentation result evaluation systems (Renard et al., 2020). In addition, there is (a) an imbalance in data availability in medical versus biomedical sciences, where significantly more datasets are available for the latter and are often designed for specific experiments (however, often without expert annotation and/or gold standards); and (b) even though there are efforts to make DL methods more accessible, typical biomedical scientists typically require support and expertise from computer scientists to apply and modify DL methods. Due to these challenges, we take the opportunity to integrate and compare conventional image analysis and DL methods in this overview to facilitate the understanding and potential uptake in an interdisciplinary fashion. We appreciate that the concepts and terminology of ML and DL are complex and recommend relevant literature to readers (Chicco, 2017; Greener, Kandathil, Moffat, & Jones, 2022; van Iterson, van Haagen, & Goeman, 2012)

As we showcase DL from a biological application perspective, we are not focusing on the design or algorithmic assessment of performance, but instead discuss DL application to segmentation of zebrafish vascular data from a single transgenic, *Tg(kdrl:HRAS-mCherry)*^{s916}. To achieve this, networks based on three different architectures were trained to compare them against each other. Specifically, an original U-Net, SegNet, and three modified U-Nets (dU-Net1-3) were trained on a dataset using ground truth segmented masks obtained after SE (Fig. 7A-C; see Materials and Methods for details). The resulting trained network is then applied to the evaluation dataset. Two popular DL network architectures were chosen, the original U-Net (Ronneberger et al., 2015) and SegNet (Badrinarayanan et al., 2017). U-Net was developed specifically for segmenting biomedical images, whereas SegNet was developed for generic image segmentation. Both have shown promising results in many applications of semantic segmentation. However, employing the network architecture directly to new data is often insufficient to produce effective segmentation.

Due to its wide applicability, the original U-Net architecture provides a good starting point, and modifications can make this more suitable to specific tasks, such as the segmentation problem of the zebrafish brain vasculature, (called dU-Net; see Materials and Methods). A DL network can be optimized for a specific task in various ways; here, (i) the original U-Net architecture was made deeper by adding more convolutional layers [i.e., the overall architecture—the number of layers and nodes—is best decided empirically (Brownlee, 2018)]; (ii) batch normalization was employed (i.e., standardize layer inputs for each mini batch), and (iii) dropout procedures were applied (i.e., temporary removal of nodes during the training process). Together, these optimizations were aimed to avoid overfitting, where the network performs well only on the training data but not test data (Abdar et al., 2021).

As for the other segmentation tests, results of DL-based segmentation approaches should first be assessed visually and compared to the gold standard; here, SE-based segmentation (Fig. 7D-H; example 3D renderings are provided in Videos 3-7) was used to assess global issues such as over- or undersegmentation.

By comparing multiple DL segmentations against SE-based segmentation as a gold standard, segmentation results can be quantitatively assessed against each other. One such quantitative comparison can be achieved by evaluating the Dice coefficient that compares image similarity between segmentation methods (where 0 indicates no overlap and 1 indicates perfect overlap). For our use case, this means a comparison between SE-based segmentation and the respective DL segmentation. This shows that (a) Dice coefficient measurement is applicable to the data under

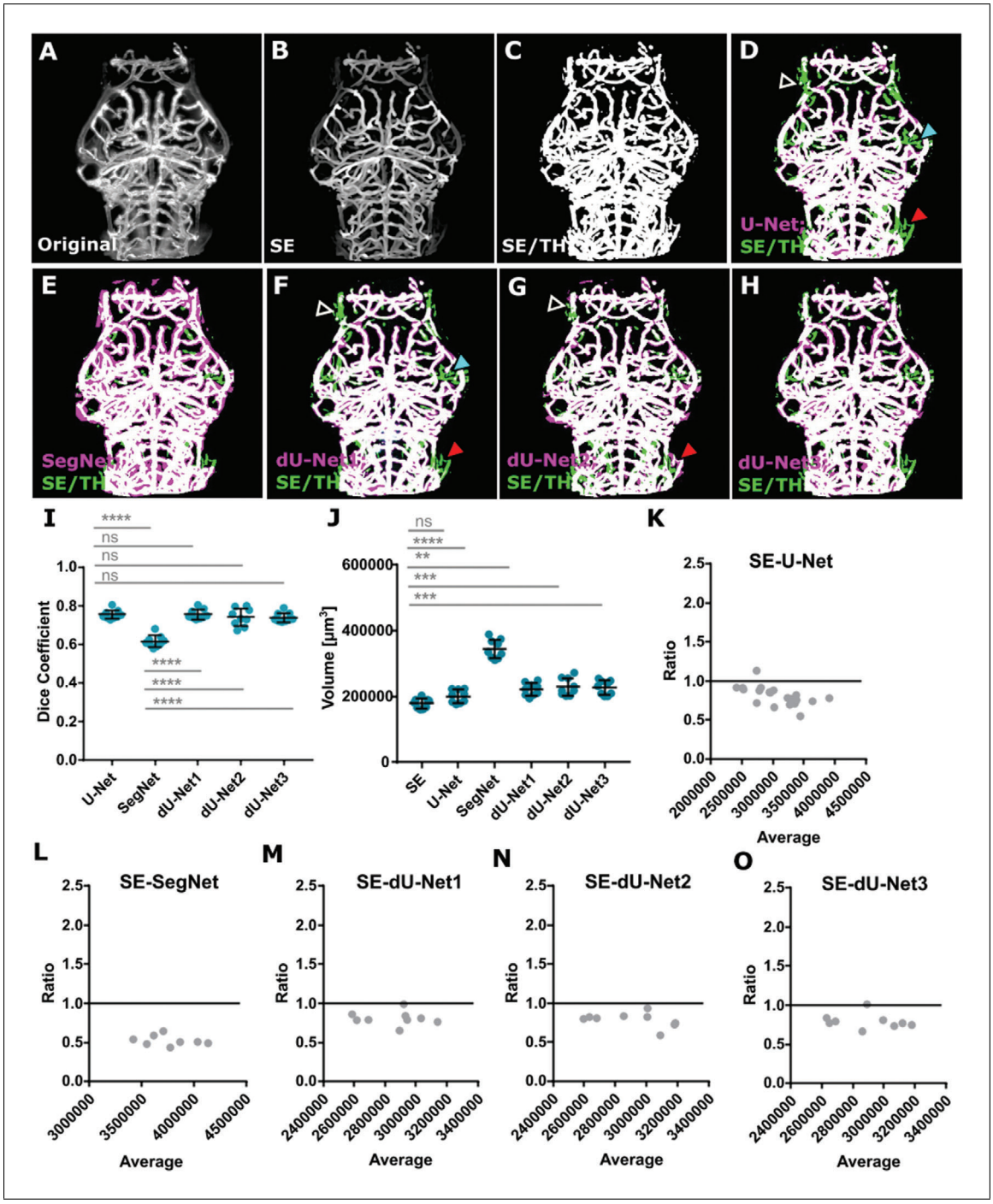

Figure 7 Deep learning results when trained from original data. (**A**) Original image, (**B**) enhanced, and (**C**) segmented using Otsu thresholding (referred to as SE/TH). (**D**) MIP of SE/TH (green) and original U-Net (magenta) segmentation, showing high degrees of overlap (white), whereas certain vessels were extracted with SE but not U-Net (arrowheads). (**E**) MIP of SE/TH (green) and SegNet (magenta) segmentation, showing consistent oversegmentation with SegNet. (**F**) MIP of SE/TH (green) and dU-Net1 (magenta) segmentation, showing high degrees of overlap (white), whereas certain vessels were extracted with SE/TH but not dU-Net1 (arrowheads). (**G**) MIP of SE/TH (green) and dU-Net2 (magenta) segmentation. (**H**) MIP of SE/TH (green) and dU-Net3 (magenta) segmentation. (**I**) Dice coefficient of segmentation outcomes (n = 9; 3 dpf). (**J**) Quantified vascular volumes. (**K-O**) Bland-Altman ratio test comparing vascular volume values.

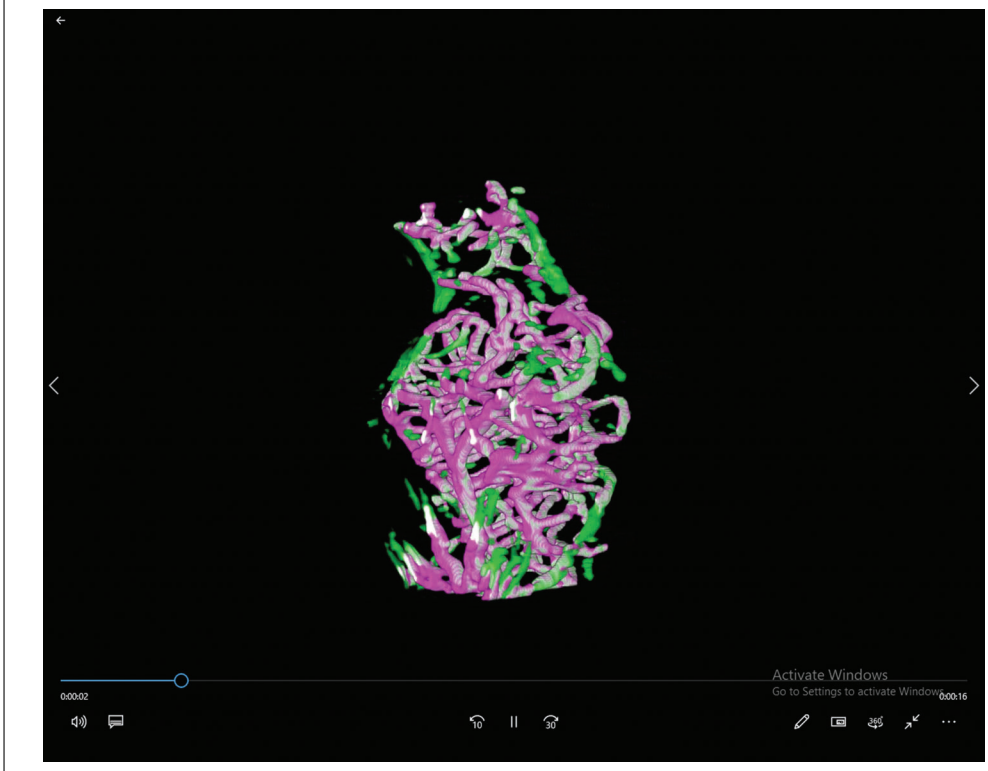

Video 3 3D rendered segmentation results of U-Net. Video shows 3D rendered 3 dpf *Tg(kdrl:HRAS-mCherry)*^{s916} after SE-based segmentation (green) and U-Net segmentation (magenta).

examination and (b) that U-Net architectures deliver better results than SegNet (Fig. 7I). Next, the vascular volume can again be used as a segmentation accuracy measure. Here, SegNet is found to deliver over-segmentation, as shown by significantly higher vascular volumes than in the other approaches (Fig. 7J; Table 1). Lastly, Bland-Altman testing can provide further insights (where 1 indicates high agreement), as it is a method to assess measurement agreements (Bland & Altman, 1986). Applying this method to our use case again shows that U-Net architectures deliver better results than SegNet, in agreement with the above assessments (Fig. 7K-O).

In addition to segmentation accuracy, workflow handling is also an important consideration. For example, the DL approaches discussed operate in 2D on a slice-by-slice basis with a 1-2 s segmentation time (after training) per slice (~400-700 slices per stack), resulting in typical run times between 7 and 23 min for segmenting a full stack. In contrast, SE-based segmentation performs in 3D and typically requires approximately 50 min in total per stack, a significant time benefit in favor of DL.

In summary, DL approaches are promising alternatives to conventional image processing methods for vasculature segmentation, with U-Net-based architectures performing particularly well. Using visual assessment, together with Dice coefficient measurements, vascular volume quantification, volume CoV analysis, and Bland-Altman ratio analysis are valid approaches to assess, compare, and describe segmentation approaches and aid validation.

WIDER IMPLICATIONS

Although this review has focused on segmentation of the zebrafish brain vasculature, many concepts and principles discussed here apply to other data. Such wider applications include the following:

- Using simulated tubes could be beneficial to other tube-like structures such as lymphatic vessels or certain neuron data.
- Experimental and computational alteration of the CNR is widely applicable to any data acquired with optical microscopy.
- Data with known large biological effect sizes can be used as a first assessment

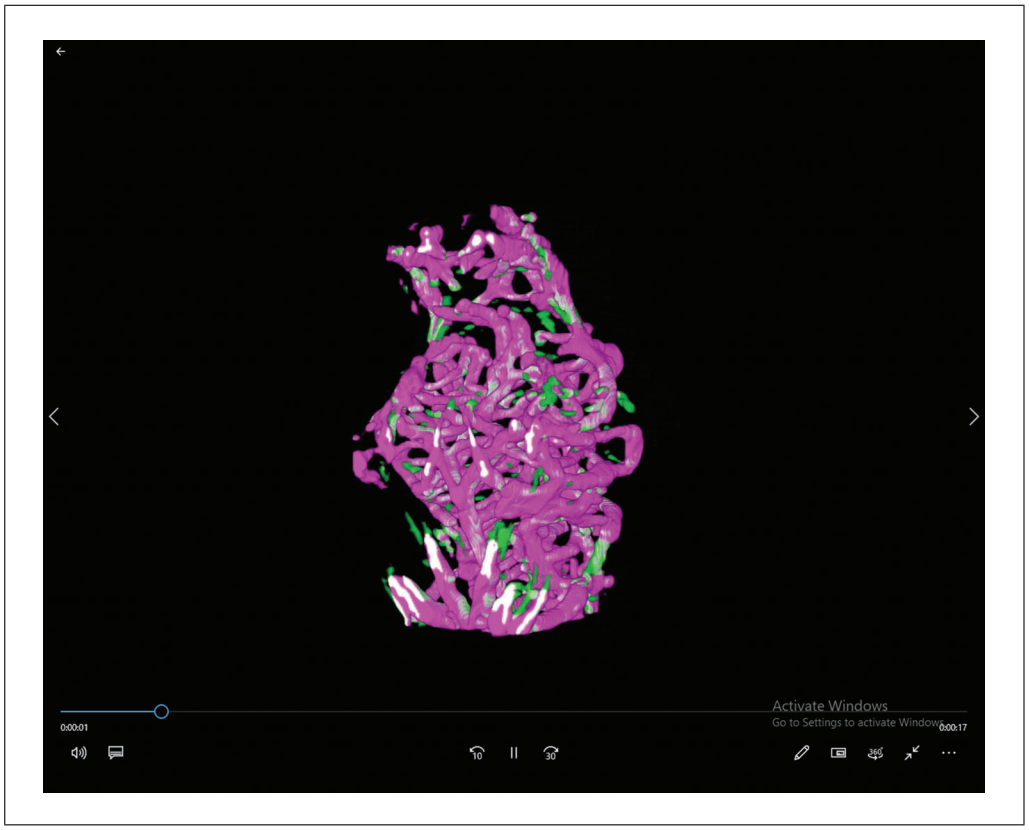

Video 4 3D rendered segmentation results of SegNet. Video shows 3D rendered 3 dpf *Tg(kdrl:HRAS-mCherry)*^{s916} after SE-based segmentation (green) and SegNet segmentation (magenta).

of segmentation and quantification performance, as shown by exsanguination; this is also applicable to animals without blood flow [such as *tnn2a* morphants (Sehnert et al., 2002)] or any other severe phenotypes.

Detection of smaller biological effect sizes can take advantage of the differences between developmental stages as shown here and used previously (Daetwyler et al., 2019), or between groups treated using drugs with known vascular effects [such as anti-VEGF treatment to inhibit vascular growth (Kugler et al., 2022)].

Double-transgenic or dual labeling can be used to assess segmentation and improve segmentation outcomes, as previously shown for the mouse brain vasculature (Todorov et al., 2020).

However, although many principles can be generalized and adapted, fine-tuning is often needed for applications other than the one for which a workflow was developed, including analysis of different vascular beds and imaging modalities (Moccia et al., 2018). This same principle is valid when applying a segmentation approach to other vascular-like cell types (e.g., lymphatics) or other organisms.

In terms of segmentation validation of the zebrafish brain vasculature, the following aspects need to be considered for adaption to other datasets:

a. The zebrafish vasculature is an enclosed circulatory system, whereas higher vertebrates have blind-ended vascular trees. Theoretically speaking, this should not alter the segmentation outcomes, but it still requires consideration.
b. Blood vessels in embryonic zebrafish show a low size variation in the µm range, whereas human vessel scales can range from µm to cm. Thus, it is likely that multiscale enhancement approaches may be required in some cases, although few current imaging modalities image across this range.
c. We showed that thorough investigation of a segmentation approach enables its application to lumenized and unlumenized vessels within the same image, with similar signal distributions being conserved in other vertebrates (Kugler et al., 2018; Todorov et al., 2020). However, immunohistochemical methods often introduce speckles or

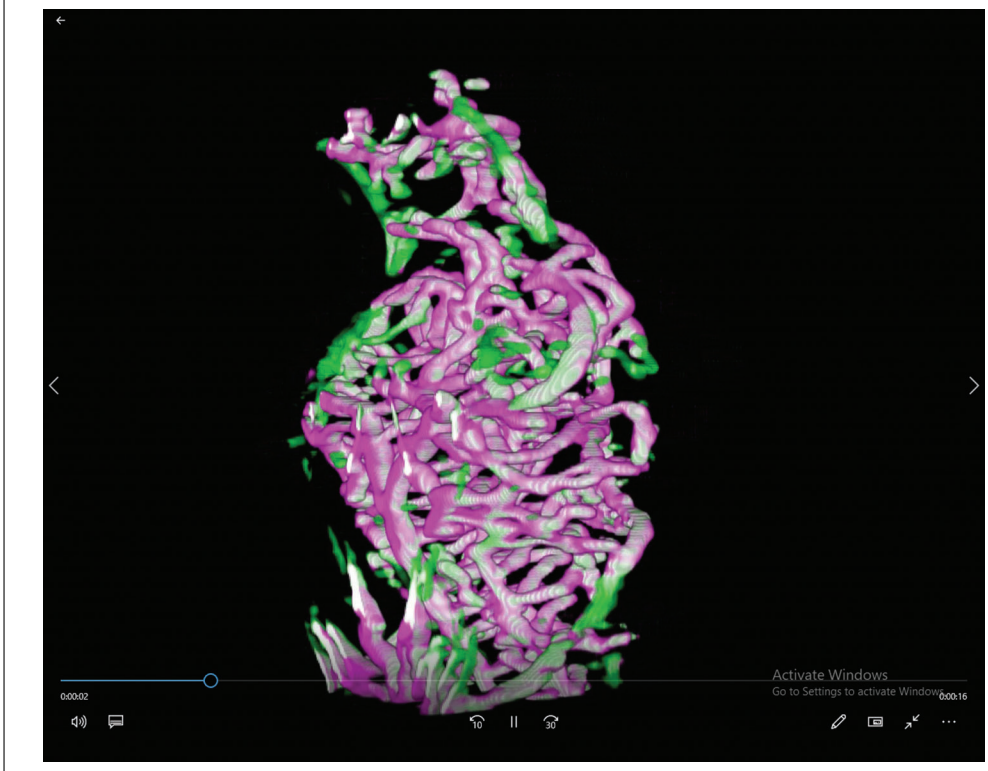

Video 5 3D rendered segmentation results of dU-Net1. Video shows 3D rendered 3 dpf *Tg(kdrl:HRAS-mCherry)*^{s916} after SE-based segmentation (green) and dU-Net1 segmentation (magenta).

blobs that require removal, for example, by connected component analysis after segmentation.

d. Our work has focused on data acquired in transparent embryos up to 5 dpf. However, for data acquired in older nontransparent samples or other vertebrates, tissue clearing may be required for visualization of the brain vasculature. It was previously shown that vascular segmentation and analysis remain valid following tissue clearing (Kirst et al., 2020; Lindsey, Douek, Loosli, & Kaslin, 2018; Miyawaki et al., 2020; Todorov et al., 2020).

CONCLUDING REMARKS

In this work, steps toward developing and validating a segmentation workflow were demonstrated, with the zebrafish brain vasculature as a use case. Our overview covered various techniques to validate the robustness, sensitivity, and accuracy of segmentation workflows, including synthetic tubes, experimental data, and augmented experimental data, paired with comparative approaches. For studying enhancement and segmentation, FWHM is appropriate to quantify local vessel diameters in the data examined here, similar to data acquired with medical imaging modalities (Merkx et al., 2012; Varma, Subramanyan, & Durgan, 2004). Furthermore, we discussed visual and quantitative assessments (e.g., CoV, Dice coefficient, and Bland-Altman ratio) of segmentations with general and DL approaches.

Segmentation Validation and Benchmark Datasets

Using manual measurements, comparisons of segmentation methods, and purpose-built datasets (i.e., varying CNR levels, exsanguination, development, and double transgenics), an objective way to examine and validate segmentation workflows can be established. Considering that phantom models and segmentation benchmarks are still widely lacking in biomedical sciences, a multilevel validation approach is a meaningful way to deliver reliable biomedical image analysis workflows. Together, this overview provides a proof of principle on how experimental, simulated, and analytical approaches can be combined to assess analysis workflows in biomedical image analysis, as was previously shown for medical image analysis (Kirişli et al., 2013). Once

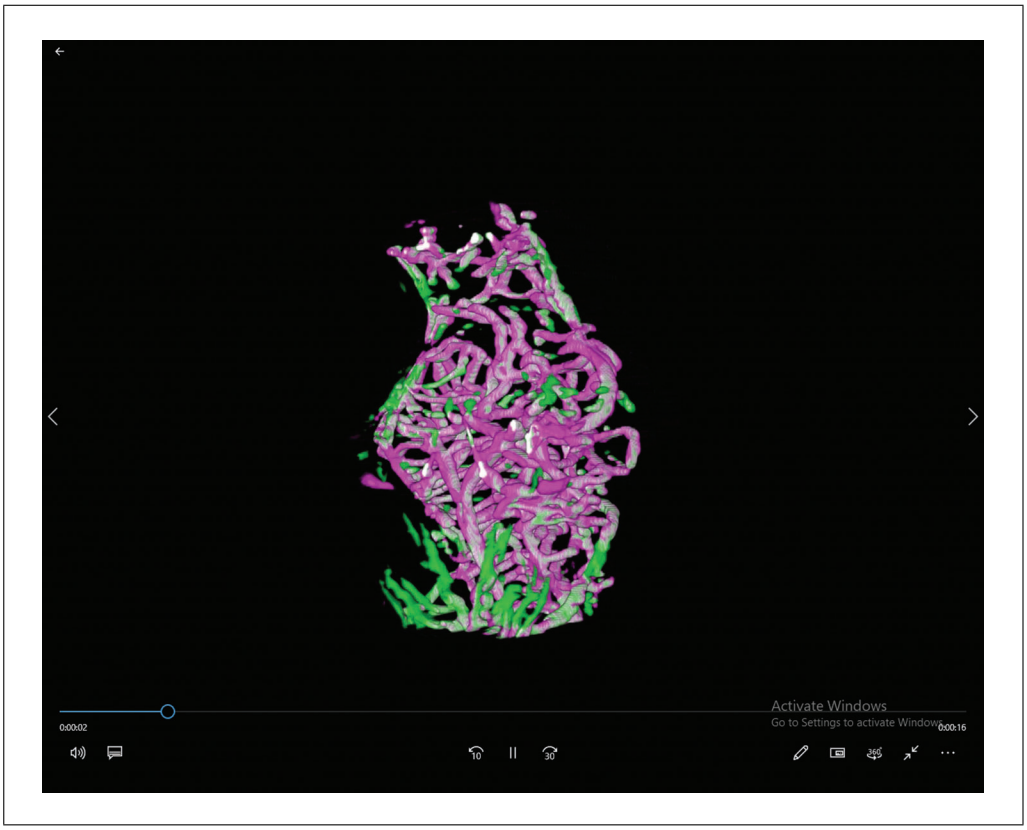

Video 6 3D rendered segmentation results of dU-Net2. Video shows 3D rendered 3 dpf *Tg(kdrl:HRAS-mCherry)*^{s916} after SE-based segmentation (green) and dU-Net2 segmentation (magenta).

such segmentation validation is established, this allows these measurements to be used as benchmarks to test against other enhancement and segmentation workflows. However, application to other ages, vascular beds, visualization techniques, or species will require further optimization.

Segmentation Transferability to Other Visualization Techniques in Zebrafish Embryos

As most segmentation workflows are developed for one specific reporter line, segmentation transferability to other transgenic reporter lines requires further attention, as transferability studies have never been conducted. Using the concept of double transgenics or double markers is a valuable approach for examining segmentation outcomes as well as identifying/confirming optimal markers. For example, in our use case, we found that nonvascular signals (pan-endothelial) as well as nonspecific (e.g., skin) signals lead to a quantifiable increase in the extracted vascular volume. These examples show that direct segmentation transferability is unlikely but that improvements are required, and these could be at various levels such as image preprocessing to enhance vascular and decrease nonvascular signals, exclusion of unconnected components, exclusion of objects under a specified size threshold, or exclusion based on the peripheral position. Similarly, DL approaches can take advantage of advances in the field of transfer learning, where previously optimized networks are efficiently retrained for additional applications.

Future work could build on this by (a) studying data visualized with microangiography (*in vivo*, visualizing only perfused vessels) or immunohistochemistry (fixed tissue, visualizing whole vasculature), or (b) examining data acquired with other techniques, such as confocal microscopy [significant signal decay along the z axis (Tröger et al., 2020)]. Importantly, even though SE was developed for MRI data, transferability to transgenic reporter line data acquired with LSFM does exist. Thus, there is no reason to believe that it cannot be further optimized to data with similar properties such as lymphatics or other networks with tubular structures.

DL-based segmentation

Overall, although DL-based segmentation delivered good segmentation outcomes, segmentation validation steps showed that there

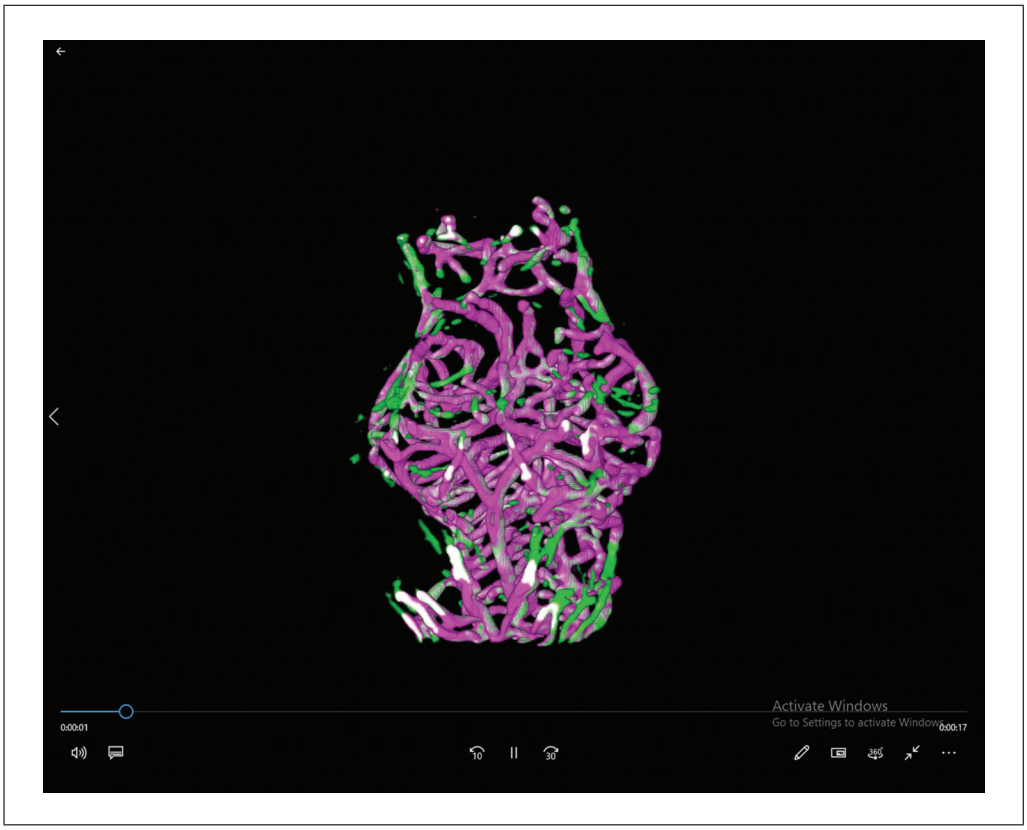

Video 7 3D rendered segmentation results of dU-Net3. Video shows 3D rendered 3 dpf *Tg(kdrl:HRAS-mCherry)*^{s916} after SE-based segmentation (green) and dU-Net3 segmentation (magenta).

Table 1 Dice Coefficient and Jaccard Index of ML-Based Segmentation Approaches in Comparison to SE-Based Segmentation

	UNet	*SegNet*	*dU-Net1*	*dU-Net2*	*dU-Net3*
Dice Coefficient	0.754 ± 0.023	0.616 ± 0.030	0.755 ± 0.025	0.740 ± 0.046	0.739 ± 0.024
Jaccard Index	0.606 ± 0.031	0.445 ± 0.032	0.607 ± 0.033	0.589 ± 0.058	0.587 ± 0.031

was a tendency toward systematic overestimation of the vascular volume, highlighting that segmentation validation is pivotal. We demonstrate in this overview that although, or maybe even because, DL is a widely emerging field, more work is needed that examines segmentation validation, and that end-user interpretation is needed to assess the suitability for segmentation applications to everyday data.

However, even if a segmentation approach is optimized or trained on a particular dataset, transferability to other datasets should not be assumed. Thus, further work is needed to examine the performance of DL-based segmentation on datasets across samples at different ages, in different transgenic lines, and in images with varying image qualities.

In conclusion, we studied zebrafish cerebrovascular segmentation methods and provided approaches to validate the segmentation workflows in the absence of a gold standard. Using simulated, experimental, and augmented datasets allowed us to demonstrate segmentation accuracy, sensitivity, and robustness. Building on this, we could establish that a segmentation workflow optimized for a specific visualization approach (e.g., particular reporter line or antibody staining) has limited generalizability, and optimization for its application to other data is critical. Lastly, the use of different DL networks showed that a comparative approach using quantitative assessments enables segmentation validation.

Importantly, the application of robust objective segmentation allows for the reduction of the sample size needed to assess the vascular phenotype, which is important from an ethical as well as a computational point of view.

ACKNOWLEDGMENTS

This work was funded with an Imaging and Modelling Node Studentship from the Department of Infection, Immunity, and Cardiovascular Disease at the University of Sheffield, as well as a Bridging Fund from the Insigneo Institute for In silico Medicine (The University of Sheffield), awarded to E.K. The Zeiss Z1 light sheet fluorescence microscope was funded by a British Heart Foundation Infrastructure Award IG/15/1/31328 granted to T.C.

Funding bodies had no involvement in the study design, or in the collection, analysis, and interpretation of the data.

The authors are grateful to the funders for supporting this project. The authors thank Professor Holger Gerhardt, Dr. Robert Wilkinson, and Dr. Aaron Savage for the provision of transgenic lines.

The authors dedicate this work to Dr. Andrik Bin Rampun, who brought new perspectives and always did so with a smile.

AUTHOR CONTRIBUTIONS

Elisabeth C. Kugler: conceptualization, data curation, formal analysis, methodology, project administration, software, validation, visualization, writing original draft, writing review and editing; **Andrik Rampun**: methodology, software, writing original draft; **Timothy J.A. Chico**: conceptualization, funding acquisition, project administration, resources, supervision, visualization, writing review and editing; **Paul A. Armitage**: conceptualization, funding acquisition, methodology, project administration, resources, supervision, writing review and editing.

CONFLICT OF INTEREST

The authors declare no conflict of interest.

DATA AVAILABILITY STATEMENT

Example data were shared as appropriate at zenodo.org: Simulated Tubes and Filter Responses (doi: 10.5281/zenodo.5898012), Decreasing Contrast-To-Noise Ratio (doi: 10.5281/zenodo.5910316), Exsanguination (doi: 10.5281/zenodo.5914725), and Development (doi: 10.5281/zenodo.5914749).

LITERATURE CITED

Abdar, M., Pourpanah, F., Hussain, S., Rezazadegan, D., Liu, L., Ghavamzadeh, M., … Nahavandia, S. (2021). A review of uncertainty quantification in deep learning: Techniques, applications and challenges. *Information Fusion*, *76*, 243–297. doi: 10.1016/j.inffus.2021.05.008.

Badrinarayanan, V., Kendall, A., & Cipolla, R. (2017). SegNet: A deep convolutional encoder-decoder architecture for image segmentation. *IEEE Transactions on Pattern Analysis and Machine Intelligence*, *39*, 2481–2495. doi: 10.1109/TPAMI.2016.2644615.

Bland, J. M., & Altman, D. G. (1986). Statistical methods for assessing agreement between two methods of clinical measurement. *Lancet*, *1*, 307–310. doi: 10.1016/S0140-6736(86)90837-8.

Bowley, G., Kugler, E., Wilkinson, R., Lawrie, A., van Eeden, F., Chico, T. J. A., … Serbanovic-Canic, J. (2021). Zebrafish as a tractable model of human cardiovascular disease. *British Journal of Pharmacology*, *179*, 900–917. doi: 10.1111/bph.15473.

Brownlee, J. (2018). How to configure the number of layers and nodes in a neural network. Available at: https://machinelearningmastery.com/how-to-configure-the-number-of-layers-and-nodes-in-a-neural-network/.

Chang, J.-M., Huynh, N., Vazquez, M., & Salafia, C. (2013). Vessel enhancement with multiscale and curvilinear filter matching for placenta images, pp.125–128. In *2013 20th International Conference on Systems, Signals and Image Processing (IWSSIP)*.

Chen, Q., Jiang, L., Li, C., Hu, D., Bu, J., Cai, D., & Du, J. (2012). Haemodynamics-driven developmental pruning of brain vasculature in zebrafish. *PLoS Biology*, *10*, e1001374. doi: 10.1371/journal.pbio.1001374.

Chi, N. C., Shaw, R. M., De Val, S., Kang, G., Jan, L. Y., Black, B. L., & Stainier, D. Y. R. (2008). Foxn4 directly regulates tbx2b expression and atrioventricular canal formation. *Genes & Development*, *22*, 734–739.

Chicco, D. (2017). Ten quick tips for machine learning in computational biology. *BioData Mining*, *10*, 35. doi: 10.1186/s13040-017-0155-3.

Chico, T. J. A., & Kugler, E. C. (2021). Cerebrovascular development: Mechanisms and experimental approaches. *Cellular and Molecular Life Sciences*, *78*(9), 4377–4398. doi: 10.1007/s00018-021-03790-1.

Chico, T. J. A., Ingham, P. W., & Crossman, D. C. (2008). Modeling cardiovascular disease in the zebrafish. *Trends in Cardiovascular Medicine*, *18*, 150–155. doi: 10.1016/j.tcm.2008.04.002.

Corliss, B. A., Mathews, C., Doty, R., Rohde, G., & Peirce, S. M. (2019). Methods to label, image, and analyze the complex structural architectures of microvascular networks. *Microcirculation*, *26*, e12520. doi: 10.1111/micc.12520.

Daetwyler, S., Günther, U., Modes, C. D., Harrington, K., & Huisken, J. (2019). Multi-sample SPIM image acquisition, processing and analysis of vascular growth in zebrafish. *Development*, *146*(6), dev173757. doi: 10.1242/dev.173757.

Feigin, V. L., Norrving, B., & Mensah, G. A. (2017). Global burden of stroke.

Circulation Research, *120*, 439–448. doi: 10.1161/CIRCRESAHA.116.308413.

Frangi, A. F., Niessen, W. J., Vincken, K. L., & Viergever, M. A. (1998). Multiscale vessel enhancement filtering, pp. 130–137. In *Medical image computing and computer-assisted intervention—MICCAI'98*. Springer.

Frangi, A. F., Niessen, W. J., Hoogeveen, R. M., van Walsum, T., & Viergever, M. A. (1999). Model-based quantitation of 3-D magnetic resonance angiographic images. *IEEE Transactions on Medical Imaging*, *18*, 946–956. doi: 10.1109/42.811279.

Gebala, V., Collins, R., Geudens, I., Phng, L.-K., & Gerhardt, H. (2016). Blood flow drives lumen formation by inverse membrane blebbing during angiogenesis in vivo. *Nature Cell Biology*, *18*, ncb3320. doi: 10.1038/ncb3320.

Greener, J. G., Kandathil, S. M., Moffat, L., & Jones, D. T. (2022). A guide to machine learning for biologists. *Nature Reviews Molecular Cell Biology*, *23*, 40–55. doi: 10.1038/s41580-021-00407-0.

Gut, P., Reischauer, S., Stainier, D. Y. R., & Arnaout, R. (2017). Little fish, big data: zebrafish as a model for cardiovascular and metabolic disease. *Physiological Reviews*, *97*, 889–938. doi: 10.1152/physrev.00038.2016.

Huisken, J., Swoger, J., Del Bene, F., Wittbrodt, J., & Stelzer, E. H. K. (2004). Optical sectioning deep inside live embryos by selective plane illumination microscopy. *Science*, *305*, 1007–1009. doi: 10.1126/science.1100035.

Khan, M. W. (2014). A survey: Image segmentation techniques. *International Journal of Future Computer and Communication; Singapore*, *3*, 89–93. doi: 10.7763/IJFCC.2014.V3.274.

Kirbas, C., & Quek, F. (2004). A review of vessel extraction techniques and algorithms. *ACM Computing Surveys*, *36*, 81–121. doi: 10.1145/1031120.1031121.

Kirişli, H. A., Schaap, M., Metz, C. T., Dharampal, A. S., Meijboom, W. B., Papadopoulou, S. L., … van Walsum, T. (2013). Standardized evaluation framework for evaluating coronary artery stenosis detection, stenosis quantification and lumen segmentation algorithms in computed tomography angiography. *Medical Image Analysis*, *17*, 859–876. doi: 10.1016/j.media.2013.05.007.

Kirst, C., Skriabine, S., Vieites-Prado, A., Topilko, T., Bertin, P., Gerschenfeld, G., … Renier, N. (2020). Mapping the fine-scale organization and plasticity of the brain vasculature. *Cell*, *180*, 780–795.e25. doi: 10.1016/j.cell.2020.01.028.

Krissian, K., Malandain, G., & Ayache, N. (1998). Model based multiscale detection and reconstruction of 3D vessels. INRIA. Available at https://hal.inria.fr/inria-00073248/document.

Kugler, E., Chico, T., & Armitage, P. (2018). Image analysis in light sheet fluorescence microscopy images of transgenic zebrafish vascular development. In M. Nixon, S. Mahmoodi, & R. Zwiggelaar (Eds.), *Medical image understanding and analysis. MIUA 2018* (pp. 343–353). Cham, Germany: Springer.

Kugler, E., Plant, K., Chico, T., & Armitage, P. (2019). Enhancement and segmentation workflow for the developing zebrafish vasculature. *Journal of Imaging*, *5*, 14. doi: 10.3390/jimaging5010014.

Kugler, E. C., Frost, J., Silva, V., Plant, K., Chhabria, K., Chico, T. J. A., & Armitage, P. A. (2022). Zebrafish Vascular Quantification (ZVQ): A tool for quantification of three-dimensional zebrafish cerebrovascular architecture by automated image analysis. *Development*, *149*(3), dev199720. doi: 10.1242/dev.199720.

Lackland, D. T., & Weber, M. A. (2015). Global burden of cardiovascular disease and stroke: Hypertension at the core. *Canadian Journal of Cardiology*, *31*, 569–571. doi: 10.1016/j.cjca.2015.01.009.

Lawson, N. D., & Weinstein, B. M. (2002). In vivo imaging of embryonic vascular development using transgenic zebrafish. *Developmental Biology*, *248*, 307–318. doi: 10.1006/dbio.2002.0711.

LeCun, Y., Bengio, Y., & Hinton, G. (2015). Deep learning. *Nature*, *521*, 436–444. doi: 10.1038/nature14539.

Legland, D., Arganda-Carreras, I., & Andrey, P. (2016). MorphoLibJ: Integrated library and plugins for mathematical morphology with ImageJ. *Bioinformatics*, *32*, 3532–3534.

Lesage, D., Angelini, E. D., Bloch, I., & Funka-Lea, G. (2008). Medial-based Bayesian tracking for vascular segmentation: Application to coronary arteries in 3D CT angiography, pp. 268–271. In *2008 5th IEEE International Symposium on Biomedical Imaging: From Nano to Macro*.

Lidayová, K., Frimmel, H., Wang, C., Bengtsson, E., & Smedby, Ö. (2017). Chapter 12: Skeleton-based fast, fully automated generation of vessel tree structure for clinical evaluation of blood vessel systems. In P. K. Saha, G. Borgefors, & G. Sanniti di Baja (Eds.), *Skeletonization-theory, methods and applications*. Cambridge, Massachusetts: Academic Press.

Lindsey, B. W., Douek, A. M., Loosli, F., & Kaslin, J. (2018). A whole brain staining, embedding, and clearing pipeline for adult zebrafish to visualize cell proliferation and morphology in 3-dimensions. *Frontiers in Neuroscience*, *11*, 750. doi: 10.3389/fnins.2017.00750.

Litjens, G., Kooi, T., Bejnordi, B. E., Setio, A. A. A., Ciompi, F., Ghafoorian, M., … Sánchez, C. I. (2017). A survey on deep learning in medical image analysis. *Medical Image Analysis*, *42*, 60–88. doi: 10.1016/j.media.2017.07.005.

Merkx, M. A. G., Bescós, J. O., Geerts, L., Bosboom, E. M. H., van de Vosse, F. N., & Breeuwer, M. (2012). Accuracy and precision of vessel area assessment: Manual versus automatic lumen delineation based on full-width at half-maximum. *Journal of Magnetic Resonance Imaging*, *36*, 1186–1193. doi: 10.1002/jmri.23752.

Miyawaki, T., Morikawa, S., Susaki, E. A., Nakashima, A., Takeuchi, H., Yamaguchi, S., … Ikegaya, Y. (2020). Visualization and molecular characterization of whole-brain vascular networks with capillary resolution. *Nature Communications*, *11*, 1104. doi: 10.1038/s41467-020-14786-z.

Moccia, S., De Momi, E., El Hadji, S., & Mattos, L. S. (2018). Blood vessel segmentation algorithms—Review of methods, datasets and evaluation metrics. *Computer Methods and Programs in Biomedicine*, *158*, 71–91. doi: 10.1016/j.cmpb.2018.02.001.

Moen, E., Bannon, D., Kudo, T., Graf, W., Covert, M., & Van Valen, D. (2019). Deep learning for cellular image analysis. *Nature Methods*, *16*, 1233–1246. doi: 10.1038/s41592-019-0403-1.

Otsu, N. (1979). A threshold selection method from gray-level histograms. *IEEE Transactions on System Man Cybernetics*, *9*, 62–66. doi: 10.1109/TSMC.1979.4310076.

Patera, A., Zippo, A. G., Bonnin, A., Stampanoni, M., & Biella, G. E. M. (2021). Brain micro-vasculature imaging: An unsupervised deep learning algorithm for segmenting mouse brain volume probed by high-resolution phase-contrast X-ray tomography. *International Journal of Imaging Systems and Technology*, *31*, 1211–1220. doi: 10.1002/ima.22520.

Pestel, G. J., Hiltebrand, L. B., Fukui, K., Cohen, D., Hager, H., & Kurz, A. M. (2006). Assessing intravascular volume by difference in pulse pressure in pigs submitted to graded hemorrhage. *Shock*, *26*, 391–395. doi: 10.1097/01.shk.0000228792.10550.ed.

Renard, F., Guedria, S., Palma, N. D., & Vuillerme, N. (2020). Variability and reproducibility in deep learning for medical image segmentation. *Scientific Reports*, *10*, 13724. doi: 10.1038/s41598-020-69920-0.

Ronneberger, O., Fischer, P., & Brox, T. (2015). U-Net: Convolutional networks for biomedical image segmentation. In N. Navab, J. Hornegger, W. M. Wells, & A. F. Frangi (Eds.), *Medical image computing and computer-assisted intervention–MICCAI 2015* (pp. 234–241). Cham, Germany: Springer International Publishing.

Sato, Y., Nakajima, S., Atsumi, H., Koller, T., Gerig, G., Yoshida, S., & Kikinis, R. (1998). 3D multi-scale line filter for segmentation and visualization of curvilinear structures in medical images. In *CVRMed-MRCAS'97* (pp. 213–222). Berlin, Heidelberg: Springer.

Savage, A. M., Kurusamy, S., Chen, Y., Jiang, Z., Chhabria, K., MacDonald, R. B., … Wilkinson, R. N. (2019). tmem33 is essential for VEGF-mediated endothelial calcium oscillations and angiogenesis. *Nature Communications*, *10*, 732. doi: 10.1038/s41467-019-08590-7.

Schindelin, J., Arganda-Carreras, I., Frise, E., Kaynig, V., Longair, M., Pietzsch, T., … Cardona, A. (2012). Fiji—an open-source platform for biological image analysis. *Nature Methods*, *9*, 676–682. doi: 10.1038/nmeth.2019.

Sehnert, A. J., Huq, A., Weinstein, B. M., Walker, C., Fishman, M., & Stainier, D. Y. R. (2002). Cardiac troponin T is essential in sarcomere assembly and cardiac contractility. *Nature Genetics*, *31*, 106–110. doi: 10.1038/ng875.

Strahler, A. N. (1952). Dynamic basis of geomorphology. *GSA Bulletin*, *63*, 923–938. doi: 10.1130/0016-7606(1952)63%5b923:DBOG%5d2.0.CO;2.

Tam, S. J., Richmond, D. L., Kaminker, J. S., Modrusan, Z., Martin-McNulty, B., Cao, T. C., … Watts, R. J. (2012). Death receptors DR6 and TROY regulate brain vascular development. *Developmental Cell*, *22*, 403–417. doi: 10.1016/j.devcel.2011.11.018.

Todorov, M. I., Paetzold, J. C., Schoppe, O., Tetteh, G., Shit, S., Efremov, V., … Ertürk, A. (2020). Machine learning analysis of whole mouse brain vasculature. *Nature Methods*, *17*, 442–449. doi: 10.1038/s41592-020-0792-1.

Tröger, J., Hoischen, C., Perner, B., Monajembashi, S., Barbotin, A., Löschberger, A., … Hemmerich, P. (2020). Comparison of multiscale imaging methods for brain research. *Cells*, *9*, 1377. doi: 10.3390/cells9061377.

van Iterson, M., van Haagen, H. H. H. B.M., & Goeman, J. J. (2012). Resolving confusion of tongues in statistics and machine learning: A primer for biologists and bioinformaticians. *Proteomics*, *12*, 543–549. doi: 10.1002/pmic.201100395.

Varma, J. K., Subramanyan, K., & Durgan, J. (2004). Full width at half maximum as a measure of vessel diameter in computed tomography angiography. In *Medical imaging 2004: Image perception, observer performance, and technology assessment* (pp. 447–454). International Society for Optics and Photonics.